ISSN 1665-8607
Bi-Annual

QUEST RJ

MISSION STATEMENT OF QUEST

"To Provide quality and state-of-the-art education (coursework, practical training and research) in prescribed branches of Engineering and Science to the enrolled students in order to make them better professionals and better human beings; so that they become capable of contributing amicably towards national development".

QUAID-E-AWAM UNIVERSITY RESEARCH JOURNAL OF ENGINEERING, SCIENCE & TECHNOLOGY

VOLUME 8 NO. 1&2 JAN-DEC-2007

Bi-annual: *ISSN 1665-8607*

Quaid-e-Awam University Research Journal of Engineering, Science & Technology

EDITORIAL BOARD

ANNUAL SUBSCRIPTION ..... Rs. 200.00 (INLAND), US$20.00 (FOREIGN, BY SURFACE MAIL)
SINGLE ISSUE..... Rs. 100.00 (INLAND), US$10.00 (FOREIGN, BY SURFACE MAIL)

The Bi-Annual Quaid-e-Awam University Research Journal of Engineering, Science & Technology, shall be supplied free of cost in exchange of Research Journal(s) from other Universities/Institutions and Research Centers.

ISSN 1665-8607

ACKNOWLEDGEMENT

The members of Editorial Board, Quaid-e-Awam University Research Journal of Engineering, Science & Technology are grateful for valuable and critical suggestions on various Research Paper(s) sent to following **Researchers/Experts** for Volume 8 No. 1&2 Jan-Dec, 2007 Issue. The members also appreciate the **Referees/Experts** for sharing their knowledge and expertise towards improvement of standard of this research Journal.

LIST OF REFEREES/EXPERTS

INTERNAL REFEREES/EXPERTS

Prof. Dr. Ali Bux Soomro,
Dean Faculty of Engineering,
QUEST, Nawabshah.

Prof. Dr. Bashir Ahmed Memon,
Civil Engineering Department,
QUEST, Nawabshah.

Associate Prof. A. Fattah Chandio,
Department of Electronics Engineering,
QUEST, Nawabshah.

EXTERNAL REFEREES/EXPERTS

Prof. Dr. Ghous Bakhsh Khaskheli,
Civil Engineering Department,
MUET, Jamshoro.

Prof. Dr. B. S. Choudhry,
Department of Electronic, Telecom & Biomedical Engineering,
MUET, Jamshoro.

Prof. Dr. Hussain Bux Mari,
Department of Industrial Engineering & Management,
MUET, Jamshoro.

Prof. Dr. Abdul Hakeem Mallah,
Department of Metallurgy & Materials,
MUET, Jamshoro.

MODELING PROPERTIES OF SELF-COMPACTING CONCRETE: AN M5 MODEL TREE BASED APPROACH

Paratibha Aggarwal*, Yogesh Aggarwal** and Dr. Mahesh Pal***

ABSTRACT

The paper explores the potential of M5 model tree based approach in predicting 28-days compressive strength and slump flow of self-compacting concrete. A total of 80 data collected from the exiting literature are used in present study. To compare the performance of the technique, prediction was also done using a back propagation neural network model. A correlation coefficient of 0.908 with a root mean square error of 5.92 for strength prediction was achieved by M5 model tree approach. In comparison, a value of 0.906 as correlation coefficient and 6.01 as root mean square error was obtained by neural network approach. For slump flow prediction, correlation coefficient values of 0.901 and 0.914 (root mean square error of 9.174 and 8.778) were achieved by M5 model tree and neural network modeling approaches respectively. Results from this study suggests a comparable performance by M5 model tree based approach to neural network approach for both strength and slump prediction. It was observed that in comparison to neural network. M5 model tree requires no user-defined parameters to be set and also involves using a small computational cost, as choice of suitable architecture has always been a problem with neural network approach and requires lot of efforts and computational cost.

Keywords: compressive strength. slump flow, prediction, M5 model tree, neural network.

1. INTRODUCTION

Concrete is one of the most versatile construction material that has been widely used for almost a century now. Concrete is fabricated from a few well-defined components i.e. cement, water, fine aggregates, and coarse aggregates. It was observed that varying these components, different types of concretes like High Performance Concrete, Ready Mix Concrete and Self - Compacting Concrete can be obtained. Some additions like plasticizers, superplasticizers, viscosity modifying agents cause the changes in the properties of concrete.

The mechanical performance and long term durability of concrete structures are greatly affected by compaction work of fresh concrete during placement at construction sites. Further, the compaction has to be compromised due to use of congested and heavily reinforced concrete structural members, the limited access of mechanical vibrators in hard to reach areas, the lack of skilled labor and the noise levels associated with mechanical vibrators. These problems were overcome by developing a new type of flowable

* Lecturer, Civil Engg. Deptt., N.I.T.Kurukshetra. India
** Lecturer, Civil Engg. Deptt., N.I.T.Kurukshetra. India
*** Astt. Prof., Civil Engg. Deptt.. N.I.T.Kurukshetra. India

concrete called Self-Compacting Concrete (SCC).

Self -Compacting concrete is defined as the type of high performance concrete, which fills all corners of formwork without vibration. It has good deformability, high segregation resistance and no blocking around reinforcement. SCC was developed initially in Japan in the 1980's (Okamura,H., [1]) and later adopted by countries like UK and other European countries. The successful development of SCC must ensure a good balance between deformability and stability .It requires the manipulation of several mixture variables to ensure acceptable rheological behavior and proper mechanical properties. Some guidelines which have been set for mixture proportioning of SCC are i) reducing the volume ratio of aggregate to cementitious material; increasing the paste volume and water-cement ratio (w/c), ii) controlling the maximum coarse aggregate particle size and total volume; and iii) using various viscosity enhancing admixtures (VEA) (Nagamoto et al. [2]). Also, absence of theoretical relationships between mixture proportioning and measured engineering properties of SCC makes it more complex. Some attempts have been made to describe these properties using traditional regression analysis tools and statistical models (Sonebi,M.,[3-4]). Neural Network have also been successfully applied to prediction of compressive strength of concrete mixes (Kasperkiewicz et al. [5]; Lie and Serra, [6]; Yeh, [7]; Hong-Guang and Ji-Zong, [8]; Dias and Pooliyadda, [9]; Ren and Zhao, [10]; Lee, [11]; Kim et al. [12]) and for prediction of performance of self-compacting concrete.

The objective of this paper is to predict the slump and compressive strength of SCC mixtures using a tree based regression methodology. MS Model Tree used in present study was proposed by Quinlan [14]. This approach is being used effectively in different civil engineering problems (Bhattacharya et al. [15]; Solomatine et al. [16- 17]) and has been found to work well in comparison to much used neural network approach. [13]

One major issue in the design of an artificial neural network is the determination of suitable architecture. A back propagation neural network based modelling algorithm requires setting up of different learning parameters (like learning rate, momentum etc), the optimal number of nodes in the hidden layer and the number of hidden layers so as to have a less complex network with a relatively better generalization capability. In most of the reported applications, selection of a number of hidden layers and the number of nodes in hidden layer is done by using a rule of thumb or trying several arbitrary architectures and selecting one that gives the best performance. Further, a suitable value of parameters like learning rate and momentum is also required for selected hidden layers and nodes. Design of a neural network involves in using non-linear optimization problem that provides a local minima. During training process a large number of training iterations may force artificial neural networks to over train, which may affect the predicting capabilities of the model. Several studies have suggested to use a validation data set (i.e. a data set other than the training data set) to have an idea about the suitable number of iterations for a specific data set. This may be a problem for studies where number of data set is limited, like concrete strength predictions. Choice of a suitable architecture has always been a problem with neural network approach and requires a lot of efforts and computational cost. Presence of local minima due to the use of a non-linear optimization problem with a back propagation neural network approach is another drawback while the advantage of using M5 model tree is its speed and requiring no user-defined parameter.

The complex relationship between mixture proportions and engineering properties of SCC is generated based on existing data in the open Literature.

2. M5 MODEL TREE

The parameter space; is split into areas (subspaces) by this technique and,it builds in each of them a linear regression model. In fact the resulting model can be seen as a modular model, or a committee machine, with the linear models being specialized on the particular subsets of the input space. Combination of specialized models ("local" models) is used in the modeling quite often. However, the M5 model tree approach is based on the principle of information theory that makes it possible to split the multi-dimensional parameter space and generate the models automatically according to the overall quality criterion. It allows for variation in the number of models created.

The splitting in M5 Modal Tree approach follows the idea of a decision tree (Figure 1), but instead of the class labels it has linear regression functions at the leaves, which can predict continuous numerical attributes. Model trees generalize the concepts of regression trees, which have constant values at their leaves (Wit ten & Frank, [19]). So, they are analogous to piece-wise linear functions (and hence nonlinear). Computational requirements for model trees grow rapidly with increase in dimensionality of the data set. Model trees learn efficiently and can tackle tasks with very high dimensionality. The major advantage of model trees over regression trees is that model trees are much smaller than regression trees and regression functions do not normally involve many variables. The working of M5 algorithm is used in the present study for inducing a model tree is described as:

Suppose a set of T training examples is available. Each example is characterized by the values of a fixed set of (input) attributes and has an associated target (output) value. The aim is to construct a model that relates a target value of the training cases to the values of their input attributes. The quality of the model will generally be measured by the accuracy with which it predicts the target values of the unseen cases. Tree-based models are constructed by a divide-and-conquer method. The set T is either associated with a leaf, or some test is chosen that splits T into subsets corresponding to the test outcomes and the same process is applied recursively to the subsets. The splitting criterion for the M5 model tree algorithm is based on treating the standard deviation of the class values that reach a node as a measure of the error at that node, and calculating the expected reduction in this error as a result of testing each attribute at that node.

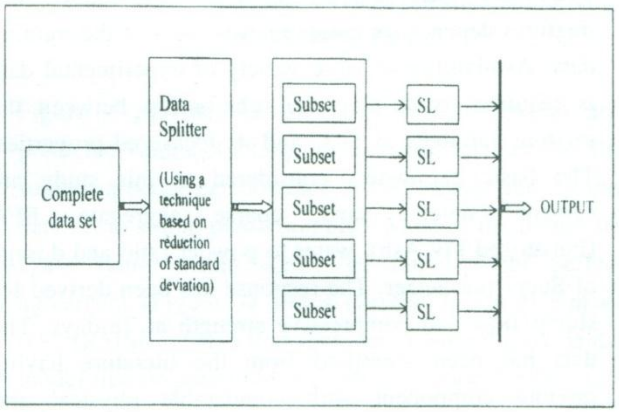

Figure 1: Architecture of M5 Model Tree

The formula to compute the standard deviation reduction (SDR) is:

$$SDR = sd(T) - \sum_{|T|}^{|T_i|} sd(T_i) \qquad (1)$$

where T represents a set of examples that reaches the node; Ti represents the subset of examples that have the ith outcome of the potential set; and sd represents the standard deviation. After examining all the possible splits, M5 chooses the one that maximizes the expected error reduction. Splitting in M5 ceases when the class values of all the instances that reach anode vary just slightly, or only a few instances remain. This division often produces a large tree like structure that must be pruned back, for instance by replacing a subtree with a

leaf. In the final stage, a smoothing process is performed to compensate for the sharp discontinuities that will inevitably occur between adjacent linear models at the leaves of the pruned tree, particularly for some models constructed from a smaller number of training examples. In smoothing, the adjacent linear equations are updated in such a way that the predicted outputs for the neighbouring input vectors corresponding to the different equations are becoming close in value.

3. DATABASE

The model's success in predicting the behaviour of SCC mixtures depends on comprehensiveness of the training data. Availability of large variety of experimental data is required to develop the relationship between the mixture variables of SCC and its measured properties. The basic parameters considered in this study are cement content, sand, coarse aggregate, PFA (Pulverised Fly Ash), water to powder ratio and dosage of Super plasticizer. The response has been derived for slump flow and compressive strength at 28-days. The data has been identified from the literature having mixture component with comparable physical and chemical properties. The exclusion of one or more of SCC properties in some studies and the ambiguity of mixture proportions and testing methods in others was responsible for setting the criteria for identification of data. Table I gives the description of the data identified from the literature.

Table 1: Source of Training data

S. #.	Source of Training data	No. of Training data	Comments
1.	Bouzoubaa and Lachemi (2001)	9	Laboratory data
2.	Ghezel and Khayat (2002)	18	Experimental data
3.	Bui et al. (2002)	14	Laboratory data
4.	Patel et al. (2004)	21	Laboratory data
5.	Sonebi (2004)	18	Laboratory data

The training of M5 modal tree was carried out using pair of input vector and output vector. The M5 model tree was designed using 69 pairs of input and output vectors for slump prediction and 80 data for strength prediction. The data sets are collected from studies by Bouzoubaa and Lachemi [20], Ghezal and Khayat [21], Bui et al., [22], Patel et al., [23] and Sonebi[3-4]. Input vector consisted of mixture variables and an output vector of one element i.e. slump flow and compressive strength at 28-days. For slump and strength prediction, the input parameters are weight of cement, sand, coarse aggregate, water-binder ratio, volume of superplasticizer and PFA. A back propagation neural network was also used to compare its performance with M5 model tree based approach. A neural network based modeling algorithm requires setting up of different learning parameters (like learning rate, momentum), the optimal number of nodes in the hidden layer and the number of hidden layers so as to have a less complex network with a relatively better generalisation capability.

4. RESULTS AND ANALYSIS

The acceptance / rejection of the model developed is determined by its ability to predict the rheological behavior and compressive strength of SCC. Also, a successfully trained model is characterized by its ability to predict slump flow and compressive strength values for the data it was trained on. A 10-fold cross validation was used to predict the slump and compressive strength for the data set used in this study. The cross validation is the method of accuracy of a classification or regression model. The input data set is divided into several parts (a number defined by the user), with each part intern used to test a model fitted to the remaining part. The correlation coefficient and root mean square error (RMSE) was used to judge the performance of M5 model tree as well as of the neural network approach in predicting the slump and strength.

Table 2 provides the correlation coefficient and RMSE obtained with this data using M5 model to predict the slump flow and 28 days compressive strength. To compare the performance of M5 model tree, graphs between actual and predicted slump flow and strength are plotted. The performance of M5 model tree based approach in predicting the compressive strength for this data set is shown in Figure 2. Results suggest that most of the points are lying within ± 20% of the line of perfect agreement, which suggest that M5 based modelling approach, can effectively be used to predict the compressive strength for self -compacting concrete data. A correlation coefficient of 0.91 (RMSE = 5.9) was achieved with this approach (Table 2).

Table 2: Summary of coefficients by Neural Network (NN) and M5 Modelling Technique (M5)

Meth-odology	Property	Correlation Coefficient	Mean Absolute Error	Root Mean Square Error
NN	Slump	0.914	7.085	8.778
	Strength	0.906	4.819	6.005
M5	Slump	0.901	7.197	9.174
	Strength	0.908	4.514	5.923

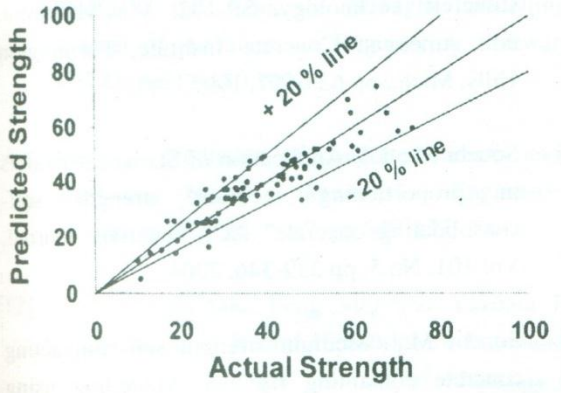

Figure 2: Actual v/s Predicted value for strength (MPa) by M5 Model Tree

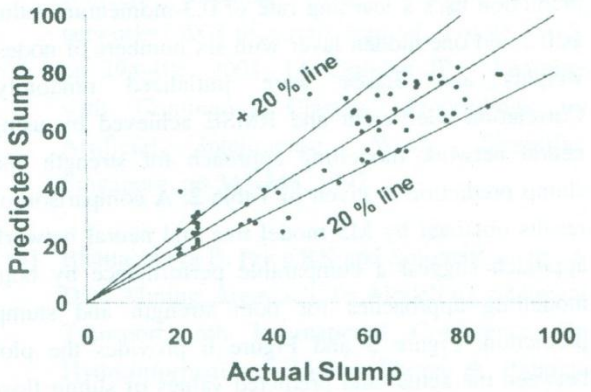

Figure 3: Actual v/s Predicted value for Slump Flow (cm) by M5 Model Tree

Figure 3 provide the plots between the actual and predicted values of slump for the used data set. Results suggest a better performance by M5 model tree for this data set in slump prediction also. Most of the points are again lying within +20% of the line of perfect agreement (Figure 3) and a correlation coefficient of 0.90 (RMSE = 9.17) was achieved. Figure 4 provide the model tree obtained for strength prediction for this data set.

M5 pruned model tree:
(using smoothed liner models)

LM1 (80/44.091%)
LM num: 1
strength =
0.2427 * cement
+ 0.2133 * PFA
-23.7963 *w/b
+0.0861 *sand
+0.0628 * coarse_agg
- 173.0945

Figure 4: M5 Model for the prediction of strength

To compare the performance of M5 model tree a back propagation neural network based modelling approach is used. An Architecture performing well for both data sets is chosen after a large number of trials. The back-

propagation neural network used for slump and strength prediction uses a learning rate of 0.3-momentum value as 0.2 and one hidden layer with six numbers of nodes; weights and biases were initialized randomly. Correlation coefficient and RMSE achieved by using neural network modelling approach for strength and slump prediction is given in Table 2. A comparison of results obtained by M5 model tree and neural network approach suggest a comparable performance by both modelling approaches for both strength and slump prediction. Figure 5 and Figure 6 provides the plot between the actual and predicted values of slump flow and compressive strength by neural network approach.

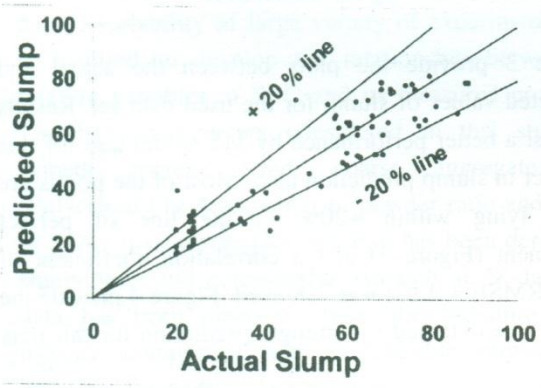

Figure 5: Actual v/s Predicted value for Slump Flow (cm) by Neural Network

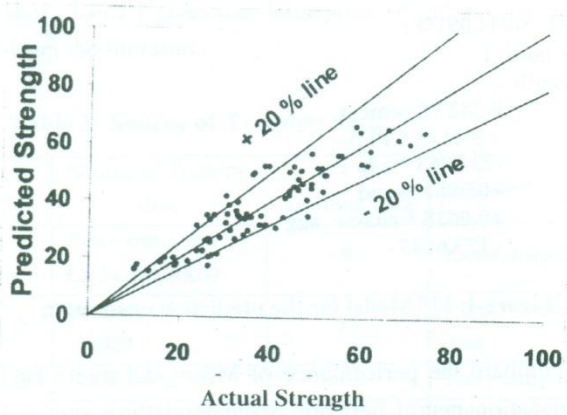

Figure 6: Actual v/s Predicted value for Strength (MPa) by Neural Network

6. CONCLUSIONS

Results from this study suggest that M5 model tree based modelling approach perform well in predicting both strength and slump flow for the data set for SCC used in present study. Further enhancement of model can be achieved by using new data developed during the actual designing of SCC mixture. The SCC mixture can be designed as per specifications, and then presented to the M5 model to predict its properties. The results obtained suggest that M5 model tree based approach can effectively be used to analyse the complex relationship between various parameters used in predicting the compressive strength and slump flow of self-compacting concrete as an alternative to neural network approach.

REFERENCES

[1] Okamura H., "Self-compacting concrete-Ferguson Lecture for 1996" Concrete International, Vol.19, No.1, pp-50-54, 1997.

[2] Nagamoto N and Ozawa K., "Mixture properties of self-compacting, High performance concrete" Third CANMET / ACI International Conference on Design and Materials and Recent Advances in Concrete Technology, SP-172, V.M.Malthotra, ed., American Concrete Institute, Farmington Hills, Mich., pp 623-627, 1997.

[3] Sonebi M., 1.1. Application of Statistical models in proportioning medium strength self-consolidating concrete" ACI Materials Journal, Vol.101, No.5, pp 339-346, 2004.

[4] Sonebi M., "Medium strength self-compacting concrete containing fly ash: Modelling using factorial experimental plans' Cement and Concrete Research, Vol.34, No.7, pp 1199-1208, 2004b.

[5] Kasperkiewicz J, Racz J and Dobarwski A., "HPC strength prediction using, artificial neural network" Journal of Computing in Civil Engineering, Vol. 9, No.4, pp 279-284, 1994.

[6] Lei S and Serra M., "Concrete strength prediction by means of neural network" Construction and Building Materials, Vol.11, pp 93-98, 1997.

[7] Yeh IC, "Design of high-performance concrete mixes using neural networks and nonlinear programming" Journal of Computing in Civil Engineering, Vol. .13, No.1, pp 36-42, 1999.

[8] Hong-Guang N and, Ji-Zong W., "Prediction of compressive strength of concrete by neural networks" Cement Concrete Research, Vol.30, No.8, pp 1245-1250,2000.

[9] Dias WPS and Pooliyadda SP., "Neural networks for predicting properties of concretes with Admixtures" Construction and Building Materials, Vol.15, pp 371-379, 2001.

[10] Ren LQ and Zhao ZY., "An Optimal Neural Network and Concrete Strength modelling" Journal of Advances in Engineering Software, Vol.33, ppI17-130,2002.

[11] Lee S., "Prediction of concrete strength using artificial neural networks" Engineering Structures, Vol. 25, No.7, pp 849-857, 2003.

[12] Kim J, Kim DK, Feng MQ and Yazdani F., "Application of Neural Networks for Estimation of Concrete Strength" Journal of Materials in Civil Engineering, Vol. 16, pp 257-264, 2004.

[13] Nehdi M, Chabib HE and Naggar MHE., "Predicting performance of self- compacting concrete mixtures using artificial neural networks.' ACI Materials Journal, VoI.98, No.5, pp 394-401, 2001. 14. Quinlan JR., "Learning with Continuous Classes.' Proceedings on Artificial Intelligence, World Scientific: Singapore, pp 343-348, 1992.

[14] Bhattacharya B, Price RK and Solomatine DP., A Data Mining Approach To Modelling Sediment Transport, 6th International Conference On Hydroinformatics - Liong, Phoon & Babovic (Eds), World Scientific Publishing Company, 2004.

[15] Solomatine DP and Dulal KN., "Model trees as an alternative to neural networks in rainfall-runoff modelling" Hydroogical Science Journal, Vol. 48 No.3, pp 399- 411, 2003.

[16] Solomatine DP and Siek MBLA., Flexible and Optimal M5 Model Trees With Applications to Flow Predictions, 6th International Conference on Hydroinformatics -Liong, Phoon & Babovic (eds), World Scientific Publishing Company, 2004.

[17] HayKin S., "Neural Networks: a Comprehensive Foundation" Macmillan, New York, 1994.

[18] Wit ten IH and Frank E., "Data Mining: Practical Machine Learning Tools and Techniques with Java Implementations" Morgan Kan Finann, San Francisco, 1999.

[19] Bouzoubaa N and Lachemi M., "Self-Compacting concrete incorporating high volumes of class F fly ash Preliminary results" Cement and Concrete Research, Vol. 31, pp 413-420, 2001.

[20] Ghezal A and Khayat KH., "Optimizing self-consolidating concrete with limestone filler by using statistical factorial design methods" ACI Materials Journal, Vol. 99, No.3, pp 264-268, 2002.

[21] Bui VK, Akkaya Yand Shah SP., "Rheological Model for self-consolidating concrete", ACI Materials Journal, Vol. 99, No.6, pp 549-559,2002.

[22] Patel R, Hossain KMA, Shehata M, Bouzoubaa N and Lachemi M., "Development of statistical models for mixture design of high-volume fly ash self-consolidation concrete" ACI Materials Journal, Vol. 101, No.4, pp 294- 302, 2004.

EFFECT OF SALINITY ON BAKED CLAY BUILDING COMPONENTS

Mahmood Memon* and Abdul Aziz Ansari**

ABSTRACT

Construction of house rather a home is the itch for which people endeavour all the entire life to let this dream come true. But it is not that simple because sky rocketing prices of construction materials and low level of income in developing countries makes it nearly impossible. However, being researchers it is our utmost responsibility to solve this problem through the use of cheaper building materials and construction processes without adversely affecting the standard and erect the houses which are elegant, durable and could sustain all the rigours of the hostile atmosphere. Therefore in order to launch a gigantic programme of investigation to check the effect of soil composition/ texture, presence of salts on the suitability of common clay for manufacture of building components which could be baked and post-reinforced with steel bars through grouting, a preliminary experimental studies were conducted. The experimental study includes determination of pH value, electric conductivity, exchangeable sodium and gypsum, total salts in solution (PPM).The physical properties of soil were also studied. These included moisture content, specific gravity, liquid limit, plastic limit, flow index, liquidity index, plasticity index, consistency index, toughness index, density of wet soil and density of dry soil. Since crushing strength of materials of construction is the major property three cubes were cast from each of the twenty five soil samples picked from various location, baked and tested for this purpose. It appears that the effect of all the above mentioned factors is negligible, because the maximum variation of cube crushing strength is only of the order of 2.8 percent. However, the strength achieved in all the cases compares well with that of concrete alluding that the material could prove a good alternative of concrete with relatively lower cost.

1. INTRODUCTION

For thousands of years clay which is abundantly available and inexpensive material has remained in extensive use not only for making pottery which includes utensils, crockery, cutlery musical instruments, jewellery but bricks, tiles and glazed tiles were made and are being made for construction of different types of structures such as buildings, bridges, abutments etc even today. Natural, non-toxic, healing, easily available, recyclable, low embodied energy, a pleasure to work with, soft and soothing, limitless creative possibilities are some of the properties of clay [1]. Traditional clay architecture is more than 10,000 years old and about one-third of world's population live in homes constructed from clay. Although it is not widely known, there are over a million buildings with clay materials in their structure in the U.K. [2]. European monasteries, castles and mansions were rendered with clay and clay was used in the infill panels of traditional timber frame houses.

* Professor Department of Civil Engineering, QUEST, Nawabshah, (Sindh), Pakistan.
** Associate Professor Department of Civil Engineering, QUEST, Nawabshah, (Sindh), Pakistan.

Many of these buildings are hundreds of years old and still standing up proudly today [3]. Over the past five years the International Resource Institute (IRI) has been working to find ways to replace all of the lumber, concrete, steel, and petroleum products used in new home construction with materials that have a decidedly lower environmental impact. The most recent sustainable architecture concept house uses a composite bentonite clay/cellulose fibre/straw-bale wall and roof system that eliminates the need for all structural lumber or steel. Ways have been found to use the cellulose/ clay composite for virtually every part of a building's structure from the foundation to structural wall components, structural skins, millwork and cabinetry [4]. The potters have attained a very high degree of competence regarding producing qualitative finished products through experience so that the manufactured goods are sufficiently dense and durable. For this purpose use is made of specially prepared clay. The process includes soaking (mixing of clay with large quantity of water) for a number of days and thumping as well as kneading properly before use. For common masonry bricks mass production is the motive rather than the quality. Therefore, common baked clay bricks are very porous and their compressive strength is only about 700 to 1300 psi when tested by placing them on edge. Bricks manufactured in mechanized plants now-a-days are quite dense and exhibit considerably higher compressive strength than manually manufactured ones. Reasonably good compressive strength can be achieved with proper compaction. When high strength is required, obviously one has to look at various parameters which might affect the strength; such as particle size of clay and silt available in natural deposits and their relative ratio, the addition of pit-sand, its ratio and grain size. In this regard preliminary experimental studies were carried out, the details of which have already been given else where [5,6]. In the first instance shrinkage, specific gravity of clay specimens and crushing strength, tensile strength, Poisson's ratio and modulus of elasticity after baking were determined. The major variable was a ratio of pit-sand and pure clay for the sake of finding the best possible combination of these two locally available materials of construction to produce sufficiently strong pre-cast post-reinforced baked clay structural members for swift erection of buildings at a lower cost than RCC without sacrificing the strength and durability. Only hand compaction was accomplished. The results were compared with those of common bricks as well. It must be mentioned that cube crushing strength as high as 25 N/mm^2 (3625 psi) was reached. Later on in continuation with this experimental work more cubes were tested which were compacted at the time of casting by applying compression force of up to 6 N/mm^2. This increased the strength up to a level of 27.61 N/mm^2 (3950 psi). During present study the effect of salinity of the soil and variety of salts and salinity of water that is used for drenching the clay is investigated.

2. AIMS, OBJECTIVES & DETAILS OF EXPERIMENTAL STUDY

A grand program was chalked out to cast pre-perforated, post-reinforced, baked clay structural panels to be used for rapid erection of buildings at relatively low cost in plain areas where the required materials for RCC are not readily available but are transported over very long distances increasing the cost of construction un-proportionately. A large number of pre-perforated clay beams have been cast, compacted by applying compression, baked, post-reinforced, grouted with cement and hill sand slurry to create bond between steel and surrounding baked clay material, cured and tested to study shear/flexure behaviour, mode of failure, crack pattern and ultimate load by applying point load, uniformly distributed load with roller supports, plate supports and fixed end boundary conditions. Details of that work are presented in reference [7].

It was deemed imperative to carry out tests on clay samples from at least 25 different sites to find the variability of contents and the effect on the fundamental

strength properties. The sites are shown in Fig: 1 (on plan of QUEST, Nawabshah). Soil Analysis was performed in terms of soil texture, salinity and sodicity status which include pH value, electric conductivity and exchangeable sodium and gypsum. Soil fertility status was also checked in terms of percentage of organic matters, percentage of nitrogen, available phosphorous and exchangeable potash for all the samples; although soil fertility is not our concern. Apart from that, weighed soil samples were also mixed with a measured quantity of water and stirred well. Then the soil was allowed to settle leaving dissolved salts in water. The water was carefully retrieved and analysis was performed in terms of pH value, electric conductivity, presence of salts of calcium, magnesium, sodium, potassium carbonate, sulphates and chlorides. It may be mentioned here that these soil samples were extracted at a depth of 4 ft from the ground level. In the laboratory at Quaid-e-Awam University of Engineering Science and Technology, Nawabshah the tests were also conducted to determine the physical properties such as natural moisture content, specific gravity, liquid limit, plastic limit, flow index, liquidity index, plasticity index, consistency index, toughness index, density of wet soil, dry density. Previously samples of underground water at QUEST, Nawabshah were tested along with other sources of water i.e. river water, water supply, sea water and LBOD (sim nala water) with particular intention to determine the hazardous effects of impurities of water on the strength of cement concrete [8].

In order to determine the fundamental strength properties (cube crushing strength) cubes of 100mm size (4 inches) were cast from all the 25 soil samples. For this purpose the soil was oven dried at 105 °C for 24 hours to extract all the moisture first. Then 20 percent water was added and mixed well in an electrically operated pan mixer. Three cubes were cast from each soil sample and compacted by applying compressive force with the help of Forney Universal Load Testing Machine. The cubes were air dried under the shade for two weeks. Then they were placed in a kiln and baked at 950 °C for 22 hours. After the discontinuation of fire the oven was allowed to cool down for two days and then the cubes were placed under the shade for other few days so that their temperature could be normal. Then the cubes were tested by applying gradual load with the help of Forney Universal Load Testing Machine.

3. RESULTS

Table 1 shows the soil analysis report for all the twenty five samples extracted from various locations. This table shows that pH value for all the samples is more than 7, implying that the soil is alkaline. Generally the soil is silty clay/loam. This simply means that there are no granular particles but only silt, clay and no silica (pit-sand). There is considerable variation of electric conductivity which is as low as 0.47 mS/cm and as high as 3.1 mS/cm. Actually EC is an indirect measurement of salinity. The higher values of EC correspond to highly saline soils. While lower values imply the absence of salts. Thus out of twenty five samples seven are highly saline, eleven are medium and the rest are non-saline. This is the point which makes it very clear that if salinity affects the over all strength of the baked clay structural panels, the variation of salinity in these samples is wide enough to exhibit itself when baked cubes are crushed. Variation of exchangeable sodium is also considerably high; the minimum value being only 0.3 (meq/100grams) and the highest value being 3.1 (meq/100grams). This is also sufficiently wide range to show its effects, if any, on the crushing strength of baked clay specimens. Here thirteen out of twenty five can be regarded as normal, seven could be termed as slightly high while only five as high. The presence of gypsum is quite low and in twenty out of twenty five samples it is zero; maximum value being 2.2. From the test results it is discerned that alkaline soil show better cohesion than those which are acidic.

Table 1 : Soil Analysis Report

Sample No.	Soil texture	Salinity and sodicity status						
	By feel Method	Ph (1:2.5)		Ec 1:2.5) ms/cm		Ex.Na meq/100 gm		Gypsum
		Value	Status	Value	Status	Value	Status	Meq/100gm
SS-1	Silty Clay Loam	7.9	Sub Alkaline	2.43	Highly Saline	1.8	Slightly High	0.0
SS-2	Silty Clay Loam	7.8	Sub Alkaline	2.60	Highly Saline	1.2	Slightly High	0.0
SS-3	Silty Clay	7.9	Sub Alkaline	1.09	Medium Saline	2.1	High	1.1
SS-4	Silty Clay	8.0	Medium Alkaline	0.60	Non saline	0.3	Normal	0.0
SS-5	Silty Clay	8.0	Medium Alkaline	0.75	Non saline	0.6	Normal	0.0
SS-6	Silty Clay	8.0	Medium Alkaline	0.67	Non saline	0.4	Normal	0.0
SS-7	Silty Clay Loam	8.0	Medium Alkaline	1.60	Medium Saline	1.2	Slightly High	0.0
SS-8	Silty Clay	8.0	Medium Alkaline	1.01	Medium Saline	0.8	Normal	0.0
SS-9	Silty Clay Loam	8.0	Medium Alkaline	1.41	Medium Saline	1.2	Slightly High	0.0
SS-10	Silty Clay Loam	8.2	Medium Alkaline	2.53	Highly Saline	2.6	High	1.6
SS-11	Silty Clay Loam	8.2	Medium Alkaline	1.12	Medium Saline	0.3	Normal	0.0
SS-12	Silty Clay	8.4	Medium Alkaline	2.33	Highly Saline	3.1	High	2.1
SS-13	Silty Clay	8.3	Medium Alkaline	3.10	Highly Saline	3.2	High	2.2
SS-14	Silty Clay Loam	7.9	Sub-Alkaline	2.13	Highly Saline	0.6	Normal	0.0
SS-15	Silty Clay	7.9	Sub-Alkaline	2.75	Highly Saline	1.9	Slightly High	0.0
SS-16	Silty Clay	8.0	Medium Alkaline	1.19	Medium Saline	0.7	Normal	0.0
SS-17	Silty Clay	8.5	Medium Alkaline	0.60	Non saline	0.8	Normal	0.0
SS-18	Silty Clay	8.2	Medium Alkaline	1.12	Medium Saline	1.8	Slightly High	0.0
SS-19	Silty Clay Loam	8.2	Medium Alkaline	0.84	Non saline	0.8	Normal	0.0
SS-20	Silty Clay	7.9	Sub Alkaline	1.12	Medium Saline	1.4	Slightly High	0.0
SS-21	Silty Clay Loam	8.3	Medium Alkaline	2.70	Highly Saline	3.0	High	2.0
SS-22	Silty Clay Loam	7.7	Sub Alkaline	1.03	Medium Saline	0.7	Normal	0.0
SS-23	Silty Clay Loam	7.7	Sub Alkaline	1.73	Medium Saline	1.0	Normal	0.0
SS-24	Silty Clay Loam	7.7	Sub Alkaline	1.46	Medium Saline	0.6	Normal	0.0
SS-25	Silty Clay Loam	7.8	Sub Alkaline	0.47	Non saline	0.4	Normal	0.0

Table 2 shows the analysis report of 16 out of 25 samples of water and Table 3 shows test reports of water only in terms of pH value, EC (mS/cm), TSS (PMM) for all the twenty five samples. It is apparent from both these tables that pH values for all the samples is more than 7. EC value varies quite a lot i.e. between 0.48 to 8.91 mS/cm clearly indicating that salinity varies widely from location to location. This clearly shows that if presence of salts effects adversely or favourably the crushing strength of baked clay specimens, it would be readily visible. Total PPM of TSS also displays a variation from a value as low as 307.2 and as high as 5702.4.

Physical properties of soil like specific gravity, Atterberg Limits, wet & dry density of all the samples determined experimentally in the laboratory are presented in Table 4.

The specific gravity of dry solids of a soil is defined as the ratio of the density of a given volume of the soil solids to the greatest density of an equal volume of pure water. The density of the substance of the soil particles is their mass per unit volume of the particles. The density of water at +4 °C is 1.000

For the purpose of structural characterization and evaluation of cohesive soils as construction materials, it is necessary to determine their consistency properties. Consistency, in general, is that property of material which is manifested by its resistance to flow. The term soil consistency conveys the idea of the degree of cohesion between the soil particles. Cohesion is the binding together of like substances by intermolecular forces and frequently, as in soils, through the medium of moisture films. In popular terms cohesion means the tendency that the soil particles exhibit in sticking together. There is a greater cohesion in the moist, fine-textured materials due the combined effect of water films (surface tension) and the physical forces that are associated with colloidal matter. Consistency pertains to cohesive soils only. Consistency is commonly described by such terms as cemented, solid, hard, brittle, stiff, sticky, plastic, mellow, or soft. Plasticity is the property which enables a material to be deformed continuously and permanently without rupture or plasticity is the ability of a body to undergo dislocation of its smallest structural particles, a consequence of the application of external forces, at ordinary temperature, without disturbance by their coherence. A soil is said to be in a plastic state when the water content is such that it can change its shape without producing surface cracks. With the increase in soil moisture, the thickness of the moisture films which surrounds the clay particles increases until at a certain state (liquid state) the cohesion is reduced so low the soil behaves as a liquid. The difference in moisture content or interval between liquid and plastic limits is termed the plasticity index. The plasticity index indicates the moisture range through which a cohesive soil has the properties of a plastic material. The plasticity index characterizes the plastic behaviour of a soil, and indicates the degree of cohesiveness of the soil. Narrower the P.I. interval is, the less plastic is the soil.

Dry density is the greatest weight per unit volume of a soil obtained by a soil compaction device at a certain moisture content and on the application of a certain compactive effort.

Mechanized plants apply a compression of 7 to 10 tons per square inch to compact the brick at a very low moisture content of 12 to 15 percent. From 2nd column of table 4, it is obvious that the moisture is between 11.41 to 17.93 percent. Therefore for structural panels when properly compacted by applying appropriate compression force, natural moisture content is enough and no extra water is needed.

Table 2 : Water Analysis Report

Sr. No.	pH	EC ms/cm 25C	Cations (meq/I)				Anions (meq/I)			
			Ca	Mg	Na Value	K	CO3	HCO3	SO4	CI
WS-1	7.6	2.76	5.4	2.4	8.4	0.2	0.0	1.5	20.1	8.5
WS-2	7.8	0.82	2.5	0.5	4.3	0.1	0.2	1.2	1.8	5.0
WS-3	7.7	1.47	3.5	1.1	7.3	0.2	0.0	2.2	1.7	11.5
WS-4	7.7	1.20	4.0	1.7	4.8	0.1	0.0	0.6	5.0	7.0
WS-5	7.7	2.90	7.7	5.1	13.8	0.2	0.0	1.2	14.4	16.0
WS-6	7.8	3.95	6.7	5.2	25.6	0.2	0.0	1.0	23.1	19.0
WS-7	8.0	2.46	3.9	1.9	15.6	0.2	0.4	1.0	13.4	12.0
WS-8	7.8	3.98	12.9	7.6	10.3	0.2	0.0	0.8	17.6	25.0
WS-9	7.8	4.06	5.3	3.9	23.5	0.6	0.0	1.5	17.3	27.5
WS-10	8.2	1.03	1.4	0.6	7.8	0.2	0.2	1.6	1.5	7.5
WS-11	7.9	4.05	7.8	2.7	24.8	0.2	0.0	1.2	28.5	16.5
WS-12	8.2	1.43	1.0	0.7	10.6	0.6	0.2	2.0	11.8	1.0
WS-13	7.9	3.28	4.8	3.7	18.4	0.2	0.0	1.6	14.2	20.0
WS-14	8.0	0.48	1.3	0.4	1.5	1.2	0.3	1.8	1.7	1.0
WS-15	7.8	1.95	6.4	1.6	10.5	0.2	0.2	1.6	13.7	5.0
WS-16	7.7	3.88	10.0	4.9	13.6	0.2	0.0	1.0	18.8	22.5

Table 3: Water Test Report.

SR. NO.	PH	E.C. mS/cm	TSS Ppm	Remarks
WS-1	8.0	0.48	307.2	Fit
WS-2	7.3	6.50	4160.0	Unfit
WS-3	7.4	5.96	3814.4	Unfit
WS-4	7.6	2.67	1708.8	Unfit
WS-5	7.8	0.82	524.8	Fit
WS-6	7.7	1.47	940.8	Marginally fit
WS-7	7.7	1.20	768.0	Fit
WS-8	7.6	4.68	2995.2	Unfit
WS-9	7.7	2.90	1856.0	Unfit
WS-10	7.8	3.95	2528.0	Unfit
WS-11	7.8	7.10	4544.0	Unfit
WS-12	8.0	2.46	1574.4	Unfit
WS-13	8.0	5.46	3494.4	Unfit
WS-14	8.0	6.27	4012.8	Unfit
WS-15	7.8	3.98	2547.2	Unfit
WS-16	7.9	6.10	3904.0	Unfit
WS-17	7.8	4.05	2592.0	Unfit
WS-18	8.2	1.03	659.2	Fit
WS-19	7.9	4.05	2592.0	Unfit
WS-20	8.2	1.43	915.2	Marginally fit
WS-21	7.9	3.28	2099.2	Unfit
WS-22	7.9	8.91	5702.4	Unfit
WS-23	7.8	1.95	1248.0	Unfit
WS-24	7.6	5.38	3443.2	Unfit
WS-25	7.7	3.88	2483.2	Unfit

Table 4: Physical Properties Of Soil Samples

Sample No.	Moisture Contents	Specific Gravity	Liquid Limit	Plastic Limit	Flow Index	Liquidity Index	Plasticity Index	Consistency Index	Toughness Index	Density of wet soil	Density of dry soil
S-01.	14.55	2.56	45.75	25.83	8.35	-0.56	19.92	1.56	2.38	1.54	1.34
S-02.	15.93	2.47	45.25	23.58	8.50	-0.23	21.67	1.35	2.54	1.55	1.34
S-03.	15.47	2.52	43.25	23.60	5.50	-0.41	19.65	1.41	3.74	1.55	1.34
S-04.	17.40	2.55	43.50	23.21	5.25	-0.28	20.29	1.28	3.86	1.55	1.32
S-05.	16.34	2.51	44.75	23.93	7.10	-0.36	20.82	1.36	2.93	1.53	1.31
S-06.	13.99	2.57	45.25	23.13	8.50	-0.41	22.12	1.41	2.60	1.53	1.34
S-07.	15.41	2.54	45.50	24.01	8.50	-0.40	21.49	1.40	2.53	1.53	1.32
S-08.	11.41	2.47	44.75	24.49	7.25	-0.64	20.26	1.64	2.79	1.53	1.37
S-09.	13.00	2.52	44.75	23.85	7.15	-0.52	20.90	1.51	2.92	1.52	1.33
S-10.	13.27	2.54	45.00	23.90	7.25	-0.50	21.10	1.50	2.91	1.54	1.35
S-11.	15.84	2.55	46.25	24.25	9.10	-0.38	22.00	1.38	2.42	1.53	1.32
S-12.	14.66	2.56	45.35	21.85	8.15	-0.30	23.50	1.30	2.88	1.52	1.32
S-13.	17.93	2.54	46.00	25.95	8.25	-0.40	20.05	1.40	2.43	1.52	1.29
S-14.	15.38	2.57	45.05	25.8	8.20	-0.54	19.25	1.54	2.34	1.56	1.35
S-15.	17.22	2.60	45.25	23.25	7.25	-0.27	22.00	1.27	3.03	1.55	1.33
S-16.	15.55	2.59	46.00	23.65	9.10	-0.36	22.35	1.36	2.45	1.52	1.32
S-17.	15.07	2.60	46.00	25.75	7.25	-0.41	25.75	1.20	3.55	1.54	1.33
S-18.	12.86	2.59	44.65	23.45	7.25	-0.49	21.20	1.49	2.92	1.53	1.35
S-19.	12.63	2.55	44.91	23.25	7.15	-0.49	21.65	1.49	3.02	1.52	1.35
S-20.	14.21	2.58	44.75	23.97	7.50	-0.46	20.78	1.46	2.70	1.50	1.31
S-21.	12.92	2.60	44.85	23.87	7.40	-0.52	20.98	1.52	2.83	1.53	1.36
S-22.	14.27	2.60	44.95	23.21	7.90	-0.41	21.74	1.41	2.73	1.53	1.34
S-23.	15.79	2.59	45.65	23.41	8.20	-0.34	22.24	1.34	2.71	1.52	1.31
S-24.	13.11	2.58	45.21	23.79	8.45	-0.49	21.42	1.49	2.53	1.52	1.34
S-25.	16.12.	2.60	44.67	23.61	7.05	-0.35	21.06	1.35	2.98	1.53	1.32

Table 5: Cube Crushing Strength of The Samples Collected From Different Site Within The Campus

Sample	Crushing Load (specimen No.1) "N"	Crushing Load (specimen No.2) "N"	Crushing Load (specimen No.3) "N"	Average Crushing Load "N"	Average Cube Crushing stress N/mm^2
Site –01	270092	271899	274609	272200	27.22
Site –02	264672	272802	273706	270393	27.03
Site –03	270996	273254	270996	271748	27.14
Site –04	269189	266931	268286	268135	26.81
Site –05	271447	270095	272351	271297	27.12
Site –06	287707	270996	267834	275512	27.55
Site –07	269641	267834	273254	270243	27.02
Site –08	272351	275964	272802	273705	27.37
Site –09	273706	277771	270996	274157	27.41
Site –10	270052	276867	271447	272788	27.27
Site –11	265576	268737	273706	269339	26.93
Site –12	270544	269189	273706	271146	27.11
Site –13	271899	269641	269189	270243	27.02
Site –14	272351	279125	272802	274759	27.47
Site –15	273706	270544	273254	272501	27.25
Site –16	272351	275512	270092	272651	27.26
Site –17	273254	272351	267834	271146	27.11
Site –18	269641	272802	274157	272200	27.22
Site –19	269189	265576	268737	267834	26.78
Site –20	272351	268737	270996	270694	27.06
Site –21	266931	267834	270092	268285	26.82
Site –22	275512	273254	271447	273404	27.34
Site –23	266479	275512	271447	271746	27.17
Site –24	275512	276867	271899	274759	27.47
Site –25	271899	270544	272351	271598	27.15
				Average	**27.23**

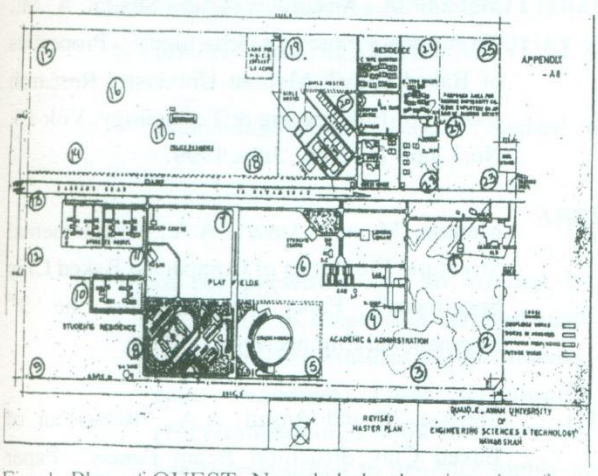

Fig. 1: Plan of QUEST, Nawabshah, showing sites from where clay samples were Picked.

Specific gravity as high as 2.60 is achieved through hand compaction. This may be compared with a value of 2.65 to 2.7 for cement concrete.

From table 4 it can be observed that there is no drastic variation of physical properties of the soil samples. This shows that although there is wide variation of the salt contents, the soil itself is sufficiently uniform at all the places. Obviously the effect of these is also found to be negligible.

Table 5 gives the details of cube crushing strength of clay specimens cast and baked from all the twenty five samples collected from different sites. From this table it is obvious that there is very small variation of average cube crushing strength from sample to sample. The maximum difference between the highest and the lowest values is 2.8 percent. For the lowest four samples the average is 26.84 N/mm^2 while for the remaining twenty one it is 27.23 N/mm^2 with an over all average of 27.16 N/mm^2 (3938 psi). This can be regarded as quite acceptable for construction of the ordinary residential buildings.

From the above discussion it is apparent that there is no pronounced effect of presence of any types of salts, pH value, EC, TSS etc on the cube crushing strength and hence presumably other fundamental structural properties of baked clay structural panels and hence the soil can be picked from any where making certain that there is no granular particles in it which are to be added at later stage in a proper proportion as already recommended in reference [5,6].

4. CONCLUSIONS

(i) The major purpose of this study was to investigate the presence of various salts and their effects on the cube crushing strength on baked clay structural panels. It is satisfying to note that this effect is almost non-extent; the maximum variation of crushing strength is only of the order of only 2.8 percent.

(ii) It was also one of the objectives to find the nature of soil and its physical composition as well as the effect on the strength properties of the final product i.e. the baked clay structural panels. Within the range of the values investigated, it is apparent that there is no drastic effect of the variation of these properties.

5. ACKNOWLEDGEMENT

Experimental work the details of which is presented in this paper was carried out in the Laboratory of the Department of Civil Engineering at Quaid-e-Awam University of Engineering Science & Tevhnology, Nawabshah. The authors acknowledge with gratitude the co-operation of Fauji Fertilizer Company Limited, Farm Advisory Centre, Nawabshah for their help and co-operation regarding the analysis of soil and water.

6. REFERENCES

[1]. N. Hendrik., "Clay Materials for self-Reliant Potter", pp. 1-31, http://Sadl.uleth.ca/nz/collect/hd/impart/gtz/g4lcle.htm

[2]. "Clay plaster", Natural Building Technology NBT Home Page, Ecology, http://natural building products couk.ntitemp.com/ecology clay.htm

[3]. "Clay", clay, Clay-Britannica concise, 2006 Encyclopaedia Britannica, Inc http://www1.eng.usm.my/Awam/info/rsoil.html

[4]. D. Lance., "Natural Composit Architecture: building without the Use of Lumber, Concrete, Steel or petroleum Products", Natural Building Colloquium, pp. 1-3, These search terms have been highlighted: Clay Material, http://216.239.59.104/search?q=cache:dfo4kxNQSWkj: www.networkearth.org/ natural bu...

[5]. Memon. M., Ansari. A. A. and Shaikh. A. M., "Preliminary Study of Structural Properties of Baked Clay", Mehran University Research Journal of Engineering & Technology, Vol. 18, No.3, pp. 161-166, July, 1999.

[6]. Memon. M. and Ansari. A.A., "Fundamental Structural Properties of Compacted Baked Clay Specimens", Paper presented in the 3rd International Engineering Congress

[7]. Memon. M and Ansari. A.A., "Behaviour of Baked Clay Structural Beam Panels", Paper submitted to CJCE-Canadian Journal of Civil Engineering, Canada. http://www.nrc.ca/cgi-bin/cisti/journals/rp/rp2_**desc_e?cjce**

[8]. Memon. M, Ansari. A.A. and Kazi., A. R., "A Study of the Effect of Aquatic Impurities on the Strength of Concrete", Journal of Engineering and Applied Science, N.W.F.P. University of Engineering & Technology, Peshawar, Vol. 18, No. 1, pp. 1-8, Jan-June, 1999.

ZONE ANNEALING AND ISOTHERMAL ANNEALING OF DISPERSION STRENGTHENED ALUMINUM ALLOYS Al20-wt%SiC AND AA3003

Muhammad Moazam Baloch*, Shakeel Ahmed Memon** and Sikandar Ali Memon***

ABSTRACT

In the present work, an attempt has been made to study the recrystallisation behaviour of dispersion strengthened aluminum alloys (Al-20 and AA3003). Two different recrystallisation treatments were applied i.e. isothermal annealing and zone annealing. Later technique was employed to investigate directional recrystallisation, a solid-state process in which heavily deformed metallic samples are recrystallised to produce highly anisotropic directional grain microstructure in a temperature gradient. Aluminum alloy AA3003 was found to be recrystallising at temperatures but directional grain growth was hindered by the pining of particles at the interface between two grains. Whereas, for alloy Al20 retardation of recrystallisation was observed which could be due to very high volume fraction of SiC particles, added to the matrix for strengthening. Microstructural investigations prior to and after deformation and after zone annealing and isothermal annealing experiments were performed using light optical microscope and transmission electron microscope. To confirm the microstructural investigations, hardness measurements were made after each successful experiment using Vicker's hardness testing machine.

Key words: directional recrystallisation, zone annealing, particle pinning, microstructure, hardness.

1. INTRODUCTION

The engineering sector is always on the look out for newer materials with superior properties combined with ease of fabrication, reproducibility and ability to play with constituents to attain a range of desired properties [1]. During research to design such materials, the concept of composite materials was developed which can bring together the combined advantages of the constituent materials not possible when they are employed alone [2,3].

The composite materials with a metal matrix are produced by casting and powder metallurgy methods. By means of casting methods composite materials reinforced by dispersion particles [4], platelets [5], non-continuous (short) fibers and continuous (long) fibers [6] as well as composite materials with hybrid reinforcement composed of particles and fibers [7] are produced. By powder metallurgy methods, composite materials reinforced by dispersion particles [8], platelets [9], non-continuous fibers and continuous fibers are manufactured [10].

* Assistant Professor, Department of Metallurgy and Materials Engineering, MUET, Jamshoro.
** Lecturer, Department of Metallurgy and Materials Engineering, Dawood College of Engineering and Technology, Karachi.
*** Assistant Professor, Department of Metallurgy and Materials Engineering, MUET, Jamshoro.

Hard particles like SiC, Al_2O_3, WC, TiC, ZrO and BC greatly improves the abrasive resistance of aluminum alloys, especially at elevated temperatures. Such composite find applications in a number of components, including impellers, pistons, piston rings, cylinder liners, connecting rods, and brake systems. They have also been tried as turbo charger impellers that run at high temperatures [11]. They merit attention because of their desirable properties including low density, high specific stiffness, reduced co-efficient of thermal expansion and increased fatigue resistance. In many stiffness-, strength-, and weight critical applications they can offer higher performance than traditional aluminum alloys at potentially lower cost [12]. The choice of silicon carbide as the reinforcement in aluminum composites is due to its excellent combination of physical properties, availability and cost. Some important properties of the Al/SiC particle composite are, the thermal expansion co-efficient can be tailored to adjoining components by adjusting the volume of reinforcement and high dimensional stability or resistance to deformation under load known as creep. The smaller the reinforcement particles the greater the strength and creep resistance [13].

The columnar grain structure or directionally recrystallised microstructure resembles that obtained by directional solidification in which the elongated columnar grains align along a particular sample axis. Most of the reported examples of directional recrystallisation are found in oxide dispersion strengthened alloys, designed primarily for their exceptional creep resistance and high temperature stability [14]. The purpose of the present work was to study the process of directional recrystallisation in dispersion strengthened aluminum alloys Al-20 and AA3003. The chemical composition of both the alloys is given in Table 1.

Table 1. Chemical composition (wt%) of dispersion strengthened aluminum alloys designated as Al20 and AA3003.

Alloy	Fe	Cu	Zr	Si	Mn	Mg	SiC	Balance
Al-20	0.7	1.25	0.1	-	-	0.95	20	Al
AA3003	0.7	0.1	0.1	0.6	1.2	-	-	Al

2. EXPERIMENTAL TECHNIQUES

2.1. MATERIAL

The alloys studied were dispersion strengthened commercial aluminum alloys designated as Al-20 and AA3003. The aluminum alloys were produced by powder metallurgy method. The powder blending route commonly used to produce metal matrix composites (MMCs) is shown in figure 1. The fabrication process involved blending pre-alloyed powder with a SiC particulate reinforcement, followed by canning, vacuum degassing at 545°C for 24 hours, and consolidated by hot isostatically pressing (HIP) to 100% density at 540°C. After consolidation the aluminum can is removed by machining and the material extruded.

The alloy Al-20 was supplied by British Petroleum. The 20wt% SiC particles have been used for reinforcement. The silicon carbide (SiC) particles had an angular morphology. Al-20 was supplied in the form of bar, with dimensions of 15mm diameter and 1000mm long. It was cold swaged down to 7.50mm diameter rod (~ 50% reduction) at ambient temperature. After cold working specimens were finally cut to a length of 20mm, using a slitting disc.

The Al-Mn alloy designated AA3003 was supplied by the Alcan International Limited, Banbury Laboratory U.K., in the form of cold rolled sheet. The cold rolling was carried out from 25mm to approximately 3.5mm (an 86% reduction)[15]. Since the alloy was supplied in

the cold rolled condition, therefore no further deformation was applied.

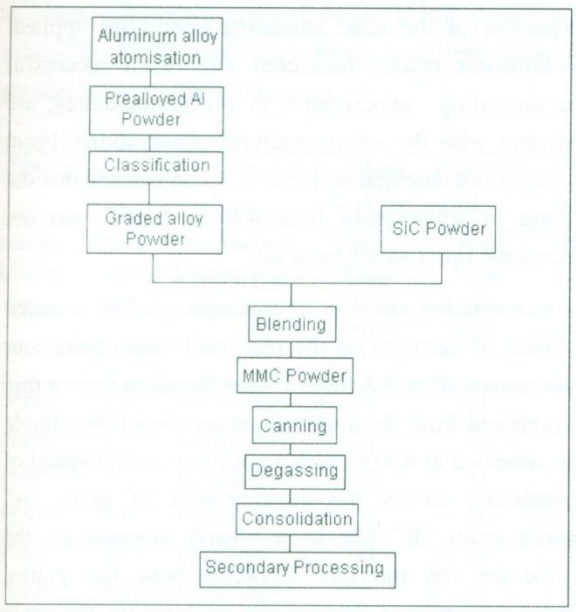

Figure 1. Flow sheet diagram illustrating the powder blending route commonly used to produce MMCs [14].

2.2. ZONE ANNEALING

Zone annealing was carried out using a crystal grower (Figure 2) as the way of achieving elongated grain structure. The specimens were placed in a silica tube, mounted on a carriage driven by variable speed electric motor. Pt/Pt-13wt%Rh thermocouple was used to measure the temperature during operation with one end of the thermocouple attached in the middle of specimen and the other end attached to Comark (a device which converts electrical potential to temperature) for measuring temperature during the movement of specimen through the R.F. Coil. To assure that every point on the specimen experienced a temperature pulse on passage through R.F. Coil the speed of the rod was controlled. After zone annealing each specimen was allowed to cool naturally in the air.

Keeping in mind, the influence of working direction on directional recrystallisation as observed during zone annealing experiments on ODS nickel base superalloy and ODS ferritic steels [16], it was thought convenient to prepare the specimens (4 x 4 x 20 mm) along the rolling direction.

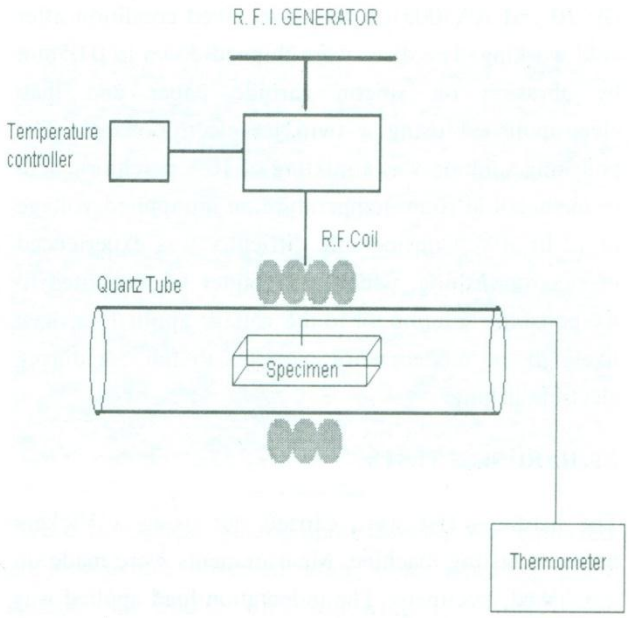

Figure 2. Diagram of crystal growth equipment adapted for zone annealing.

2.3. OPTICAL MICROSCOPY

Optical microscopy was used to observe recrystallisation in as-received, deformed and after different heat treatments. The specimens from the aluminum alloys were cold mounted in resin to avoid unnecessary heating. The specimen were then ground on silicon carbide paper to sufficient depth to remove any unrepresentative surface. After mechanically grinding down to 1200 grade emery paper, they were finally polished on a "Mastertex" final polishing cloth, using a colloidal silica polishing suspension. Mechanically polished samples were etched using a mixture of 190ml distilled water, 5ml HNO_3, 3ml HCl, 2ml HF.

2.4. TRANSMISSION ELECTRON MICROSCOPY (TEM)

A Philips EM 400 T electron microscope was used for the examination of thin foils. The operating voltage was 120 kV. Thin foil specimens were prepared for transmission electron microscopy from 0.25mm thick discs slit from dispersion strengthened aluminum alloys (Al-20 and AA3003) in the as-received condition after cold working. The discs were thinned down to 0.05mm by abrasion on silicon carbide paper and then electropolished using a twin jet electropolisher. The polishing solution was a mixture of 10% perchloric acid in methanol at room temperature, at an applied voltage of 12 to 20V. Considerable difficulty was experienced in electropolishing, which may either be attributed to the polishing solution, or to the voltage applied, or most likely to the tendency for particles to fall out during electropolishing.

2.5. HARDNESS TESTS

The hardness test were carried out using a Vickers hardness testing machine. Measurements were made on a polished specimens. The indentation load applied was 5kg. All the measurements were made at a suitable distance from the specimen edge, in order to avoid any edge effects. At least five readings were taken per specimen.

3. RESULTS AND DISCUSSION

Optical and transmission electron micrographs (figure 3 and 4) taken from the specimen in as-received condition of Al-Mn alloy AA3003, showed the expected elongated grain structure with a very low dislocation density. The particles are found randomly distributed in the matrix. The observations suggest the material went under the dynamic recovery during rolling operation.

The hardness from zone annealed samples are listed in Table 2 and the optical micrographs are shown in figures 5, 6 and 7, which were recorded after zone annealing specimens of AA3003 at T_p 430, 500 and 630°C respectively, with various zone annealing speeds ranging from 0.2, 0.4, 0.8, 1.4, 3.2, 5.0, 7.7 and 10.0 mm/min. An equiaxed grain structure was observed irrespective of the zone annealing conditions applied. The hardness results measured after each successful zone annealing experiments at the temperatures, are consistent with the microstructural observations. From the results documented in Table 2, it can be seen that the increase in temperature from 430 to 630°C, has not affected the microstructure at all.

The transmission electron microscopic studies revealed the effect of particles on the recrystallisation behaviour of aluminum alloy AA3003. Figure 8a taken from a thin foil prepared from the longitudinal section of the sample zone annealed at 430°C with a specimen travel speed of 0.2mm/min., shows the advancement of grain "A" towards grain "B" has been clearly stopped by the particle on the interface between both the grains. Another example of the particle pinning on the grain boundary is shown in figure 8b. It is presumably the pinning effect which prevents the directional growth of grains.

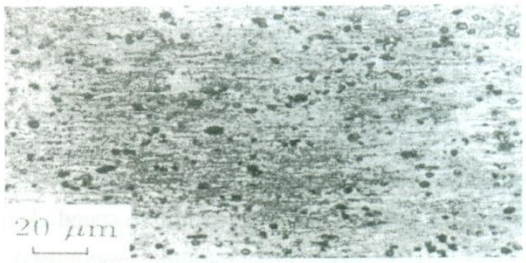

Figure 3. The as-received optical microstructure of alloy AA3003.

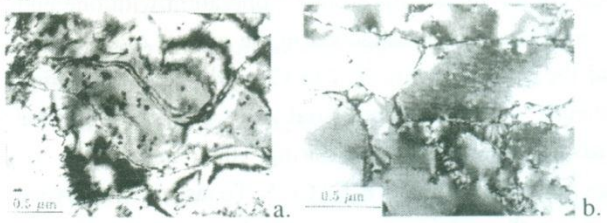

Figure 4. Transmission electron micrographs showing the microstructure of alloy AA3003 in the as-received condition. 4a. Represents the microstructure observed on a longitudinal section and 4b. represents microstructure observed on a transverse section.

Table 2. Mean hardness (averaged over five results) of samples after zone annealing. As received, AA3003 alloy has mean hardness of 67 HVN (5kg). Speed is that at which sample traverses through rf coil during zone annealing. Pl:RD indicates zone annealing direction parallel to cold rolling direction.

Zone annealing direction	Speed mm min^{-1}	As observed Microstructure	Mean Vickers Hardness with 5 kg load. Peak Temp. T_P = 430°C	Peak Temp. T_P = 500°C	Peak Temp. T_P = 630°C
Pl:RD	0.2	recrystallised	32	31	31
Pl:RD	0.4	recrystallised	31	31	31
Pl:RD	0.8	recrystallised	32	31	31
Pl:RD	1.4	recrystallised	32	31	32
Pl:RD	3.2	recrystallised	33	32	32
Pl:RD	5.0	recrystallised	32	32	33
Pl:RD	7.7	recrystallised	33	32	34
Pl:RD	10.0	recrystallised	32	32	32

The microstructure observed prior to and after deformation of aluminum alloy Al20 is shown in figure 9, and the corresponding hardness data are tabulated in Table 3. The micrographs clearly show the high volume fraction of particles and angular morphology of silicon carbide (SiC) particles.

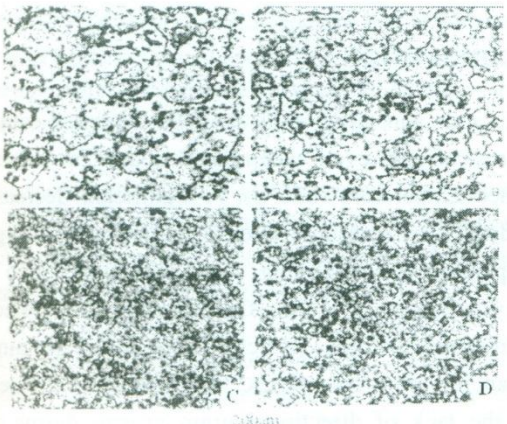

Figure 5. Optical micrographs showing the equiaxed grain structure observed after zone annealing alloy AA3003 at 430°C with following specimen travel speeds:

A. 0.2mm/min, B .0.4m/min,
C. 7.7mm/min, D. 10.0 mm/min.

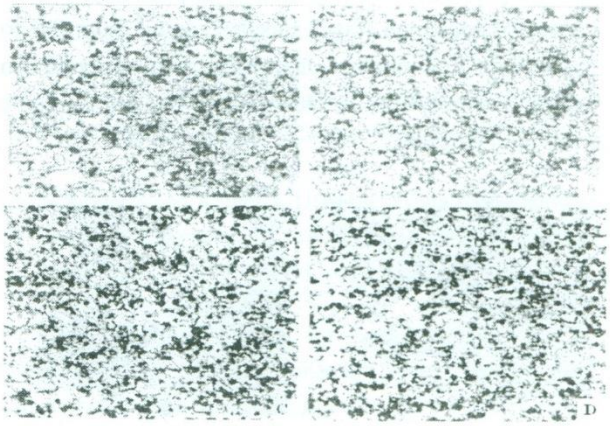

Figure 6. Optical micrographs showing the equiaxed grain structure observed after zone annealing alloy AA3003 at 500°C with following specimen travel speeds:

A. 0.2mm/min, B.0.4mm/min, C. 7.7mm/min D. 10.0 mm/min.

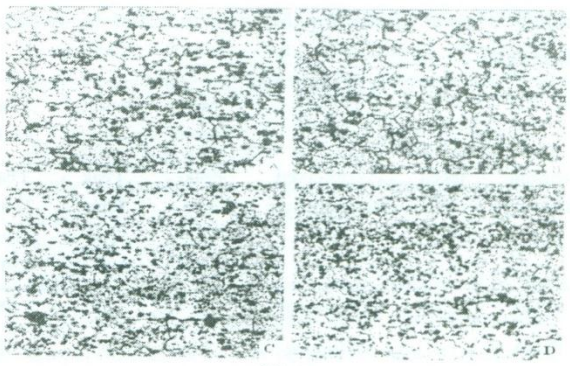

Figure 7. Optical micrographs showing the equiaxed grain structure observed after zone annealing alloy

AA3003 at 630°C with following specimen travel speeds:

A. 0.2mm/min, B. 0.4mm/min,
C. 7.7mm/min, D. 10.0 mm/min.

Optical micrographs shown in figures 10a, b and c, reveal the microstructure of alloy Al20, after zone annealing at 430, 500 and 630°C respectively, with a variety of specimen travel speeds ranging from 0.8 to 5.0mm min^{-1}. No obvious changes in grain structure can be seen, which could be due to the very high volume fraction of particles.

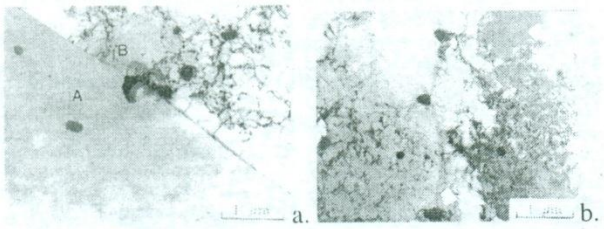

a. b.

Figure 8. Electron micrographs illustrate the pinning effect. (alloy AA3003 zone annealed at 430°C with specimen travel speed 0.2 mm/min.)

Table 3. Mean hardness (averaged over five results) of samples after zone annealing. As received and after deformation, Al20 alloy has mean hardness of 57 and 70 HVN (5kg) respectively.. Speed is that at which sample traverses through rf coil during zone annealing. Pl:SD indicates zone annealing direction parallel to swaging direction.

Zone annealing direction	Speed mm min^{-1}	As observed Microstructure	Mean Vickers Hardness with 5 kg load. Peak Temp. T_P = 430°C	Peak Temp. T_P = 500°C	Peak Temp. T_P = 630°C
Pl:SD	0.8	Deformed	58	58	58
Pl:SD	1.4	Deformed	58	59	62
Pl:SD	3.2	Deformed	59	61	59
Pl:SD	5.0	deformed	60	57	59

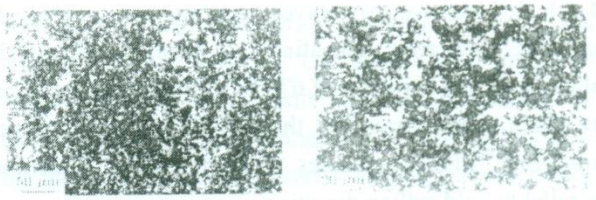

Figure 9. Optical micrographs recorded for alloy Al20, shows the microstructure of the alloy prior to and after deformation.

a. After deformation
b. As-received condition.

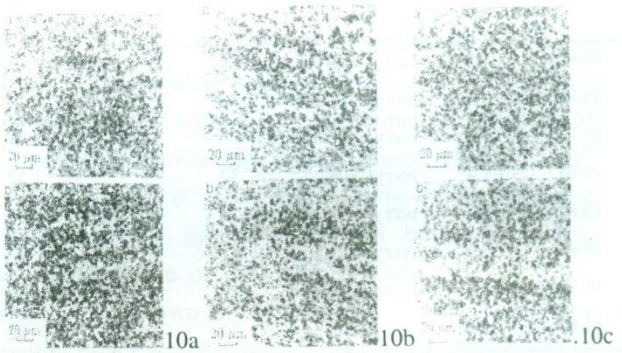

10a 10b 10c

Figure 10. Optical micrographs taken after zone annealing the samples of alloy Al20.
10a. T_P = 430°C specimen travel speeds a. 0.8mm/min and b. 5.0mm/min.
10b. T_P = 500°C specimen travel speeds a. 0.8mm/min and b. 5.0mm/min.
10c. T_P = 630°C specimen travel speeds a. 0.8mm/min and b. 5.0mm/min.

4. CONCLUSION

After zone annealing, alloy AA3003 exhibited equiaxed microstructure, even when heat treated at relatively higher temperature (630°C). A significant decrease in hardness was measured after annealing at the range of temperatures suggesting a softening due to recrystallisation. From the transmission electron microscopic studies, particles were found to pin the advancing grain boundaries, which could be the reason for the lack of directional grain growth during zone

annealing. After zone annealing, alloy Al20 exhibited considerable influence of deformed structure and high hardness values at a range of temperatures. From the microstructural observations and hardness data obtained after annealing alloy Al20, it can be concluded that due to high volume fraction of SiC particles, material cannot be easily recrystallised.

ACKNOWLEDGEMENT

The authors are grateful to British Petroleum and Alcan International Limited, Banbury Laboratory UK for supplying the alloys used in this work and to Professor D. Hull for the provision of the laboratory facilities at the University of Cambridge. Authors would also like to express their gratitude to the BCCI and CCT for their generosity in financial supporting of this project. Acknowledge is also due to Professor Dr. A. H. Mallah, for the provision of technical assistance in the Department of Metallurgy and Materials Engineering, Mehran University of Engineering and Technology, Jamshoro, Sindh, Pakistan.

REFERENCES

[1] Rupa Dasgupta and Humaira Meenai "SiC particulate dispersed composites of an Al-Zn-Mg-Cu alloy: Property comparison with parent alloy". Materials Characterisation, 54, pp., 438-445. 2005.

[2] Pitcher P.D, Shakesheff A.J and Lord J.D. "Aluminum based metal metarix composites for improved elevated temperature performance". Material Science and Technology. 14., pp., 1015-1023, 1998.

[3] Shakesheff A.J, Purdue G. "Designing metal matrix composites to meet their target: Particulate reinforced Al-alloys for missile applications". Material Science and Technology., 14, pp., 851-856. 1998.

[4] Corbin S.F and Wilkonson D.S., "The tensile properties of a particulate reinforced Al alloy in the temperature range 196 - 300°C". Canadian Metallurgical Quarterly. 35, pp., 189-198, 1996.

[5] Gupta M, Lai M.O and Soo C.Y, "Effect of type of processing on the microstructural features and mechanical properties of Al-Cu/Si metal matrix composites". Materials Science and Engineering, A210, pp., 114-122, 1996.

[6] Bowman R.R, Misra A.K and Arnold S.M, "Processing and mechanical properties of Al_2O_3 fiber-reinforced NiAl composites". Metallurgical and Materials Transactions. A 26. pp., 615-628, 1995.

[7] Schroder J and Kainer K.U, "Magnesium base hybrid composites prepared by liquid infiltration". Materials Science and Engineering A135, pp., 243-246, 1991.

[8] Abkowitz S, Weihrauh P.F and Abkowitz F.M, "Particulate reinforced titanium alloy composites economically formed by combined cold and hot isostatic pressing". Induction Heating, pp., 32-37, 1993.

[9] Kainer K.U, Schroder J and Mordike B.L, "Influence of various P/M production methods on the properties of magnesium-SiC-Composites, in L. Chandra, A.K. Dhingra (Eds), Proceedings of the International Conference on Advanced Composites 1993, TMS. pp.,1061-1065, 1993.

[10] Kaczmar J.W, Pietrzak K and Wlosinski W, " The production and application of metal matrix composite materials". Journal of Materials Processing Technology, 106, pp., 58-67, 2000.

[11] Al-Haidary J.T and Jabur Al-Kaaby A.S, "Evaluation study of cast Al-SiC_P composites". Materials Science-Poland, Vol.25, pp., 155-165, 2007.

[12] Grishaber R.B, Sergueeva A.V, Mishra R.S and Mukherjee A.K, "Laminated metal composites–High temperature deformation behavior". Materials Science and Engineering, A 403, pp., 17-24, 2005.

[13] Wei W., "High temperature MMCs for Aero-engines: Challenges and Potentials", Metals and Materials Journal, pp., 430-435, 1992.

[14] Baloch M.M, "Directional recrystallisation in dispersion strengthened alloys", Ph. D Thesis, University of Cambridge, 1989.

[15] Knowles D.M, "Fracture and fatigue in MMCs" Dissertation submitted for CPGS. University of Cambridge, 1989.

[16] Baloch M.M and Bhadeshia H.K.D.H, "Directional recrystallisation in a nickel-base ODS superalloy". Materials Science and Technology, 6, pp., 1236-1246, 1991.

ASSESSMENT OF STEADY STATE CREEP BEHAVIOUR AND MICROSTRUCTURAL INVESTIGATIONS OF MICRO-ALLOYED STEEL

Sikandar Ali Memon *, Muhammad Moazam Baloch ** and Iftikhar Ahmed Memon ***

ABSTRACT

In present work an attempt has been made to study the steady state creep characteristics of a micro-alloyed steel. The creep test conducted at 600, 700 and 800°C, in order to be within the steady state creep range, the stress level selected were below the yield stress of the material at the test temperatures. As expected the steady state creep rate increases with the increase in temperature. The microstructural investigations shown that the structure remains predominantly ferrite and pearlite with coarse grains, except at 800°C, where the structure has acquired a fine grain matrix during creep process. This may be attributed to the precipitation of micro alloyed constituents in the form of carbides having a pinning down effect of grain boundaries thus inhibiting further grain growth. The microstructure of the alloy after each test was investigated using optical microscope.

Key Words: Microalloyed steel, Creep behavior, Microstructural changes, Carbide precipitation, Pinning, Grain growth.

1. INTRODUCTION

Creep behavior and degradation of creep properties of high temperature materials are phenomena of major practical relevance. Often limiting the lives of components and structure designed to operate for long periods under stress at elevated temperatures. Because life expectancy is in reality, based on the ability of the material to retain its high temperature creep strength for a period of at least twice the projected design life [1].

The strength of metals decreases with increasing temperature. Since the mobility of atoms increases rapidly with temperature, it can be appreciated that diffusion controlled processes can have a very significant effect on high temperature mechanical properties [2]. High temperature will also result in greater mobility of dislocations by the mechanism of climb. The equilibrium concentration of vacancies like wise increases with temperature. New deformation mechanism may come into play at elevated temperature. In some metals additional slip systems are introduced with increasing temperature [3]. Another important factor to consider is the effect of prolonged exposure at elevated temperature on the metallurgical stability of metals and alloys. For example, cold-worked metals will recrystallise and under go grain coarsening [4], while the age-hardening alloys may over age and loose their strength as the second phase particles coarsen.

* Assistant Professor, Department of Metallurgy and Materials Engineering, MUET, Jamshoro.

** Assistant Professor, Department of Metallurgy and Materials Engineering, MUET, Jamshoro.

*** Lecturer, Department of Metallurgy and Materials Engineering, Dawood College of Engineering and Technology, Karachi.

Thus, it should be apparent that the successful use of metals at elevated temperatures involves a number of problems. Greatly, accelerated alloy development programme have produced a number of materials with high temperature properties, but the ever increasing demands of modern technology require materials with even better high temperature strength and oxidation resistance [5].

For a long time the principal high temperature applications were associated with steam power plants, oil refineries and chemical plants. The operating temperature in equipment such as boilers and steam turbines seldom exceeded 550°C. With the introduction of gas turbine engines, requirements developed for materials to operate in critically stressed parts, like turbine buckets, at temperatures around 850°C. The design of more powerful engines has pushed this limit to around 1000°C. Rocket engines and ballistic missile nose cones present much greater problems, which can be met only by the most ingenious use of the high temperature materials and the development of still better ones. In the last two decades, a number of new materials with improved creep resistance have been developed for long-term service at temperatures up to 600°C and above in high temperature parts of boilers, steam lines and turbines of ultra supercritical power plants [6,7,8].

For long-term application of new steels, it is necessary to assess the microstructural changes that are likely to occur during service exposure and to evaluate the effect of such changes on the high temperature creep behavior. Only with this information can the design values for components be correctly assigned. This paper examines steady state creep behavior of micro alloyed steel (GR-60) at temperatures from 600, 700 and 800°C and microstructural observations after each successive creep test are discussed.

2. EXPERIMENTAL PROCEDURE

The alloy studied was a microalloyed steel, with the commercial designation GR-60, provided by Pakistan Steel Mills Karachi. It was received in the form of billet with dimensions 100mm x 100mm x 200mm. The chemical composition of the steel investigated is presented in Table 1.

Table 1. Chemical composition of microalloyed steel GR-60.

Grade	C	Si	Mn	P	S	V	Nb	Mo	Balance
GR-60 Micro-alloyed Steel	0.28	0.15	1.1	0.035	0.035	0.04	0.04	0.04	Fe

To prepare the specimens for the creep testing, the billet was cut into square bars of 25mm x 25mm using electrically operated hacksaw cutter. Oil coolant was used to minimize over heating.

Finally, creep test specimens having dimensions shown in figure 1, were manufactured. The specimens were categorized according to the temperature of the test and the loading conditions as indicated in table 2.

Since the creep tests were to be conducted at elevated temperatures, so the specimens were loaded in correspondence with the yield stress of the material at that temperature and the cross sectional area of the specimen. The yield stress of micro alloy steel at the corresponding temperatures was obtained from F. S. Merritt's "structural steel designer's hand book" [9], and the values are listed in table 2. The specimens were tested at stress levels of 2/3 to 1/4 of yield stress values. Creep test were performed using CRL-3000 Type, creep and rupture testing machine fitted with cylindrical shaped electric furnace.

For microstructural investigations, Olympus light optical microscope fitted with camera was used and the etchant used was 2% Nital.

Table 2. Yield stress of micro-alloy steel at the corresponding temperatures, after Fedric. S. Merritt [9].

S. No	Code No of spec-imen	Code No.of Test	Temp °C	Yield Stress Tones/ in^2	Yield Stress Kg/ mm^2	Applied stress	Yielding Load Kg
1	A1	Test 1	600	15	23.25	2/3x 23.25=15.33	1203.40
2	A2	Test 2	600	15	23.25	1/2x 23.25=11.76	923.16
3	B1	Test 3	700	11.59	17.96	1/2 x 17.96= 8.98	704.93
4	B2	Test 4	700	11.59	17.96	1/3 x 17.96= 5.98	469.43
5	C1	Test 5	800	9.37	14.54	1/3 x 14.54= 4.84	379.94
6	C2	Test 6	800	9.37	14.54	1/4 x 14.54= 3.63	284.95

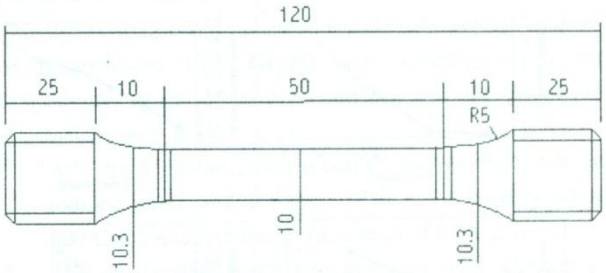

Figure 1. Dimensions of creep test specimens.

3. RESULTS AND DISCUSSION

Creep tests were conducted at 600, 700 and 800°C with two sets of stress levels at each temperature. In order to compare the results and elucidate the effect of stress and temperature on the creep characteristics the results are presented in consolidated manner in table 4 and figure 2 shows creep curves recorded, as elongation (mm) versus time in hours after each experiment at different temperatures and loading conditions.

Table 3. Comparison of results and effects of stress and temperature on the creep characteristics of Microalloyed Steel GR 60.

Specimen Identification No.	Test Temperature, °C	Stress Level	Instantaneous Steady State Creep Rate,mm/hr	Average Steady State Creep Rate, mm/hr	Remarks
A1	600	2/3 σy	0.165 (after 2 hrs)	0.15	A pronounced tertiary creep rate of 2.18mm/hr was observed after 4 hrs of test. The test ended with the fracture of the specimen.
A2	600	1/2 σy	0.15 (after 5 hrs)	0.0096	
B1	700	1/2 σy	2.23 (after 2 hrs) tertiary creep rate	1.69 tertiary creep rate	Test ended with fracture of the specimen. Testing creep rates of 2.23 mm/hr observed
B2	700	1/3 σy	0.34 (after 9 hrs)	0.31	
C1	800	1/3 σy	2.72 Z(after 5 hrs) tertiary creep rate	2.01 tertiary creep rate	The test ended with a pronounced necking of specimen. Tertiary creep rate of 2.72 mm/hrs was observed
C2	800	1/4 σy	1.09 (after 5 hrs)	0.86	

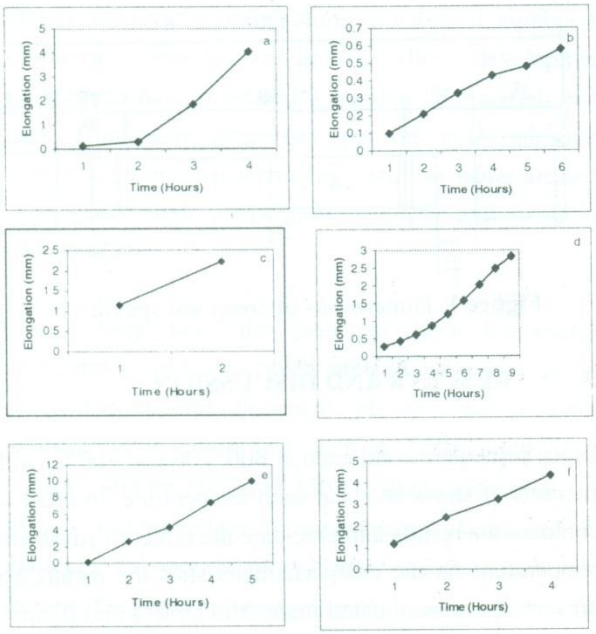

Figure 2. Shows elongation (mm) in specimens observed after each creep test at various temperatures and loading conditions. Graphs a. and b. at 600°C and two levels of applied stress 2/3σy and 1/2 σy respectively. c. and d. at 700°C and stress levels 1/2 σy and 1/3 σy, and e. and f. at 800°C and stress levels 1/3 σy and 1/4 σy respectively.

3.1. THE EFFECTS OF STRESS AND TEMPERATURE ON CREEP CHARACTERISTICS

Comparing the results at varying stress levels at the same temperatures it may be seen that at 600°C (specimen A1 and A2, represented in graphs a. and b. of figure 2), a stress level of 2/3σy subjects the specimen to tertiary creep after 2 hours and eventually fractures the specimen. Reducing the stress level to 1/2σy at the same temperature (i.e., 600°C) a steady state creep rate is observed even after 5 hours of loading. Assuming that in the first 2 hours of the test the specimen A1 exhibiting steady state condition the average creep rate recorded was 0.15mm/hr. The same for specimen A2 at a lower stress level 1/2σy was 0.0096 mm/hr. Thus at the same temperature a reduction in the stress level reduces steady state creep rate of microalloyed steel GR60.

It can also be seen from the results represented in table 3, that the sensitivity to stress level also increases with the increase in temperature. At a stress level of 1/2σy for a test at 600°C exhibits steady state creep condition where as, at the same level, at 700°C, the specimen was found to be in tertiary creep region. Therefore, it can be said that at higher temperatures material support lower stress levels so as to be within steady state region. The effect of temperature on steady state creep rates and general creep phenomenon appears to be equally significant as in the case of varying stress levels and this is graphically represented in figure 3, by plotting experimental data recorded as elongation (mm) versus temperature °C. It can be clearly seen from the figure 3 that the steady state creep rate increases significantly with the increase in temperature.

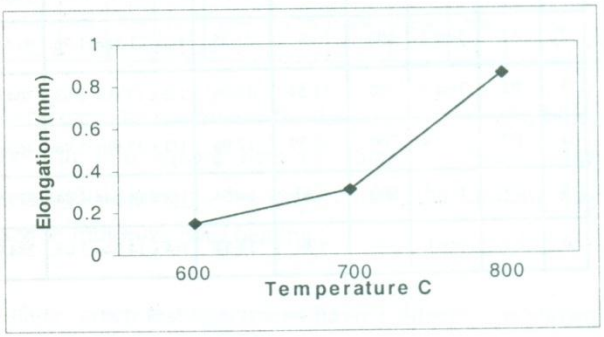

Figure 3. Shows the effect of temperature on steady state creep rate of microalloyed GR60.

3.2. MICROSTRUCTURAL ANALYSES

It is the central percept of materials science that the processing governs microstructure and that microstructure influences the properties and performance of materials. Consequently, characterization and visualization of microstructure are of considerable importance in materials research [10]

In microalloyed ferrite–pearlite steels, strength increases are primarily achieved through increase of the pearlite volume fraction or by grain refinement [11], and precipitation strengthening of the ferrite matrix as controlled with microalloy additions (e.g., Al, Nb, or Ti for grain size control and V for precipitation strengthening [12]). While the grain refinement is beneficial to both strength and toughness, the presence of pearlite limits the maximum obtainable toughness [13]. For the long-term applications of the microalloyed steels, it is necessary to assess the microstructural changes that are likely to occur during service exposure and to evaluate the effect of such changes on the high temperature

creep behavior. Only with this information can the design values for the components be designed. Figure 4 shows the microstructure recorded for various specimens. It can be seen clearly that the optical microstructure recorded in as received condition (figure 4a) of GR-60 steel consist of ferrite and pearlite structure. The lowest temperature at which the creep test was performed (i.e., 600°C) no marked difference in grain size was observed, and the material exhibited similar ferrite and pearlite microstructure (figure 4b).

Figure 4. Shows the micrographs recorded (a.) in as-received condition, (b.) after creep test performed at 600°C, (c.) after creep test performed at 700°C and, (d.) after creep test performed at 800°C.

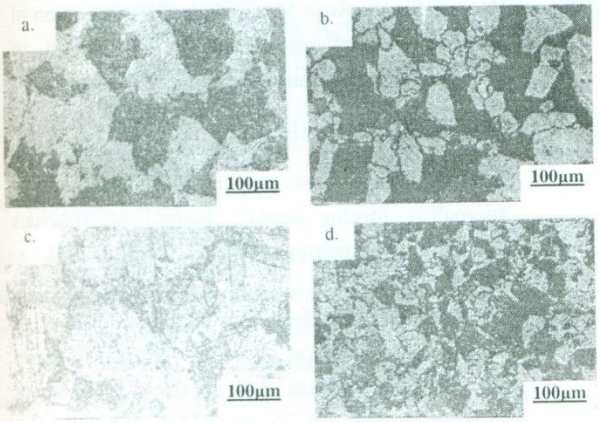

At relatively higher temperature (i.e., 700°C) grain coarsening is evident from the microstructure recorded (figure 4c). But as the creep test carried out at 800°C and the microstructure recorded after the test as shown in figure 4d, exhibited an appreciable amount of grain refinement, however, with the predominance of ferrite and pearlite phases. This grain refinement can be attributed to the precipitation of third phase particles at higher temperature, having a particle pinning effect on the grain boundaries leading to the formation of sub-grains.

Few of the microstructural changes that occur as the result of creep suggest a contribution to increased resistance to creep strain. Some reduction in grain size results from the early stages of dislocation rearrangement and during certain stages of creep loading, the precipitation of new phases might create new barriers to dislocation movement.

4. CONCLUSION

The steady state creep behavior and microstructural changes of microalloyed steel GR-60 were investigated in the temperature range of 600 to 800°C, and the following conclusions were drawn:

1. At a stress level of 2/3σy at 600°C, the material exhibited tertiary creep, and a similar behavior was observed at 800°C at a much reduced stress level of 1/3σy.
2. The steady state creep rate increases with increase in temperature. Thus an average creep rate of 0.0096mm/hr was observed at 600°C and 0.86mm/hr at 800°C.
3. During microstructural investigations, grain refinement was observed at 800°C. This may be attributed to the micro alloy contents of the steel (GR-60) to form carbides. The carbides may have precipitated at 800°C, having a pinning effect on the grain boundaries and resulted in the formation of sub-grains.

FURTHER SUGGESTIONS

In order to confirm above assumptions it would be interesting to study in detail the carbide formation and the nature of carbides, the presence of new phases at different temperatures, the effect of particles on the grain boundaries and dislocation concentration occur during creep at different temperatures using scanning electron microscope.

ACKNOWLEDGEMENT

The authors are grateful to the Principal Institute of Materials Science Pakistan Steel Mills Karachi, Professor Moinuddin Ali Khan for the provision of microalloyed steel (Gr-60) for the present study. Special thanks are due to Professor Dr. A. H. Mallah, Chairman Department of Metallurgy and Materials Engineering, Mehran University of Engineering and Technology, Jamshoro, for provision of laboratory facilities in the department.

REFERENCES

[1] V. Sklenicka et al, " Long-term creep behavior of 9 – 12% Cr plant steels", Materials Characterization, 51 pp. 35-48, 2003.

[2] Yu W, Cold-formed steel design, 3rd ed. New York, USA; John Wiley & Sons, pp., 55-60, 2000.

[3] Feng M, Wang YC, Davies JM, "Structural behaviour of cold-deformed thin-walled short steel channel columns at elevated temperatures", Part 1: Experiments, Thin-Walled Structures, 41(6), pp., 543-570, 2003.

[4] Baloch M.M, Bhadeshia H.K.D.H, "Directional recrystallisation in a nickel-base ODS superalloy", Materials Science & Technology, 6, pp.,1236-1246, 1991.

[5] Jung H.L, Mahen M, Penti M, "Prediction of mechanical properties of light gauge steels at elevated temperatures", Journal of Constructional Steel Research, 59, pp., 1517-1532, 2003.

[6] Kern T.U, Staubli M, Mayer K.H, Escher K, Zeiler G, " The European effort in development of new high temperature rotor materials up to 650°C – COST 522", Proceedings of the International Conference on Materials for Advance Power Engineering, ed. Lecomte-Beckers J, Carton M, Schubert F, Ennis P.J., Liege, Belgium: Forschungszentrum Julich; pp., 1049-1064, 2002.

[7] Staubli M et al, "Development of creep resistant sat steels within the European collaboration in advanced steam turbine materials for ultra efficient, low emmision steam power plant", Proceedings of the International Conference on Materials for Advance Power Engineering, ed. Lecomte-Beckers J, Carton M, Schubert F, Ennis P.J., Liege, Belgium: Forschungszentrum Julich; pp., 1065-1080, 2002.

[8] Fujita T, "Advances in 9-12 Cr heat resistant steels for power plant", Proceedings of 3rd Conference on Advances in Material Technology for Fossil Power Plants, ed. Viswanathan R, Baker W.T, Parker J.D. The Institute of Materials, London, UK., pp., 33-65, 2001.

[9] Feddric S.M, Structural Steel Designer's Handbook, pp. 125, 1989.

[10] Harpeet Singh, Arun M. Gokhale, "Visualization of three-dimensional microstructures", Journal of Material Characterization, 54, pp., 21-29, 2005.

[11] Matlock D. K, Krauss G, Speer J.G, "Microstructures and properties of direct-cooled microalloy forging steels", Journal of Materials Processing Technology, 117, pp., 324-328, 2001.

[12] Hasan Karabulut, Suleyman Gunduz, "Effect of vanadium content on dynamic strain ageing in microalloyed medium carbon steel", Journal of Materials and Design, 25, pp., 521-527, 2004.

[13] Jahazi M, Eghbali B, " The influence of hot forging conditions on the microstructure and mechanical properties of two microalloyed steels", Journal of Materials Processing and Technology, 113, pp., 594-608, 2001.

MATHEMATICAL ANALYSIS OF DESIGN PARAMETERS IN CDMA DOWNLINK NETWORK

M. Irfan Anis*, M. Zamin Khan**, and M. Jawwad Paracha***

ABSTRACT

This paper focuses on the analysis of design parameters in CDMA (code division multiple access) downlink (base station to mobile) network. A useful framework is provided in order to determine the optimal length for the Single Cell and Multicell network. It is not necessary, as commonly believed that to increase capacity in CDMA network it is imperative to increase number of cells in it. Explicit expressions of the capacity have been derived. Simulation, based on parameters, which enables a quick evaluation of feasibility that may be used for capacity allocation for the optimization of CDMA downlink network.

Keyword: CDMA, Single Cell, Multi Cell, Downlink, Uplink

1. INTRODUCTION

CDMA is a second generation digital mobile phone standards which takes a defferent approach from the other, competing standards: GSM, TDMA where GSM and TDMA divide the available bandwidth into "Channels" using a combination of frequency bands and time-slices, CDMA spread the signal over a wide bandwidth identifying each channel using unique digital codes. This means it can provide greater bandwidth efficiency, and have a greater potential number of channels.

CDMA presents some unique features that are not present in traditional TDMA and FDMA systems. In CDMA; all users operate on the same frequency channels at the same time. Using CDMA completely eliminates the concept of conventional frequency reuse because the same frequency can be deployed in all cells.

2. PERFORMANCE ANALYSIS

2.1 SNR (SIGNAL TO NOISE RATIO)

One problem with many digital communication systems is that the performance of the system in fine, up to some critical channel noise level, above which the system fails very quickly. This problem leads to drop outs in the signal, decreasing the reliability of the system. To be intelligible, any data that's transmitted by any means, electronic or otherwise, must rise above any accompanying noise. The measure of that intelligibility is called its signal-to-noise ratio. A wireless signal dissipates at a significant rate – it's inversely proportional to the square of the distance traveled as it radiates outward in all directions. SNR determines the link quality thus the ability to estimate SNR is important for determining suitable transmitter powers or received signal levels. SNR at a receiver is important for determining coverage and quality of service in a wireless communication system.

2.2 CAPACITY

The capacity of a CDMA System is limited by the reverse link. The reverse link uses uncorrelated, non-orthogonal PN (Pseudo Noise) codes, which makes it

* Department of Electronics Engineering, Sir Syed University of Engineering & Technology Pakistan

limited by interference from other users. Channel capacity, shown often as "C" in communication formulas, is the amount of discrete information bits that a defined area or segments in a communications medium can hold. In Direct Sequence Spread Spectrum (IX44) Cellular each user is provided with an individual and distinctive spread spectrum pseudo noise (I',V) code. As in all A-trt spwudi~zg techniques, the narrow band message signal is multiplied by the spread spectrum pseudo-noise PA; and then transmitted. Because f'N codes are uncorrelated with each other, many users can transmit at the same time and in the same radio bandwidth, then we- have universal frequency reuse. This has the consequence that there is no need for a mobile to change its frequency when moving into another cell, so we have also Soft Handoff [1].

Estimating the system capacity, it is customary to assume that the perfect power control is in place in the up link, and the down link power is the same at every base station. Under these circumstances, the interference power received at a Base Station (BS) of a given cell can be estimated by knowing the number of users in the cell (intra cell interference(, and the number of users and their locations in the neighboring cells (inter-cell interference).

The cell capacity of a CDMA system is dependent on the bandwidth. The highest error-free data rate supported in any communication system is well governed by the channel capacity formula. In a perfect noiseless environment where the signal to noise ratio (SNR) is infinite, the cannel capacity will be infinite. However, in a real world system, it is not the case. By evaluating user's SNR at various location and applying the channel capacity formula, one is able to see if the peak data advertised in the proposal is supported and to what extend it is supported [2].

2.3 INTERFERENCE

Interference is the major limiting factor in the performance of cellular radio system. Source radio system. Source of interference include another mobile in the same cells, a cell is progress in a neighboring cell, other BS operating in the same frequency band or any non-cellular system, which inadvertently leaks energy into the cellular frequency band. Interference on voice channels causes cross talk, where the subscriber hears interference in the background due to an undesired transmission. It is a well-known fact that the capacity of a CDMA cellular mobile system is determined by the interference associated with it. In a multi-cell (or sector) system this interference consists of intra-cell interference generated within the cell and inter-cell interference arranging from neighbor cells.

3. DISCUSSION

3.1 CAPACITY DERIVATION FOR SINGLE AND MULTI CELL

Assume L as length, I as total interference, P as Path Loss between Base Station and User, σ^2 as Variance, μ as Rate and γ as decaying. The Capacity of Downlink CDMA is given as [3].

$$C(a) = \frac{1}{L}\sum_{p=0}^{La-1}\int_{aL/2}^{aL/2} Log_{\,2}\left(1 + \frac{Pe^{-\gamma\|u\|}(E(\|h\|^5))^2}{I + \sigma^2 E(\|h\|^2)}\right)du \tag{3.1}$$

$$I = aP(E(\|h\|^2))^2 \sum_{i=0,i\#p}^{\frac{1}{a}-1} e^{-\gamma|u+(p-i)La|} + aPe^{-\gamma|u|}(E(|h|^4)) - (E(|h|^2))^2$$

$$C(a) = \frac{1}{L}\sum_{p=0}^{La-1}\int_{aL/2}^{aL/2} Log_{\,2}\left(1 + \frac{Pe^{-\gamma\|u\|}}{I + \sigma^2}\right)du \tag{3.2}$$

$$I = aP\sum_{i=0,i\#p}^{\frac{1}{a}-1} e^{-\gamma|u+(p-i)La|} + aPe^{-\gamma|u|}$$

Where: i=0 and i= $(\frac{1}{a}-1)$

$$I = aP\left[e^{-\gamma|u+pLa|} + e^{-r\left|u+\{p-(\frac{1}{a}-1)\}\right|La}\right]$$

$$I = aP\left[e^{-\gamma|u|}e^{-r|pLa|} + e^{-r|u|}e^{-r|\{p\}La|}e^{r|L|}e^{-r|La|}\right]\frac{(1-e^{rLa})}{(1-e^{rLa})}$$

$$I = \frac{aP}{(1-e^{rLa})}\left[e^{-ru}e^{-rpLa}(1+e^{rL}e^{-rLa})\right](1-e^{rLa})$$

$$I = \frac{aP}{(1-e^{rLa})}\left[e^{-ru}e^{-rpLa}(1-e^{rLa}+e^{rL}e^{-rLa}-e^{rL-rLa+rLa})\right]$$

$$I = \frac{aP}{(1-e^{rLa})}\left[e^{-ru}e^{-rpLa}(1-e^{rLa}+e^{rL-rLa}-e^{rL})\right]$$

$$I = \frac{aP}{(1-e^{rLa})}\left[e^{-ru}(e^{-rpLa}-e^{rL\bar{a}rLa}+e^{rL^{rLa}-rpLa}-e^{rL-rpLa})\right]$$

$$I = \frac{aP}{(1-e^{rLa})}\left[e^{-ru}e^{-rpLa}-e^{ru}e^{-rLa\,p-1)}+e^{-ru}-e^{r(\frac{1}{a}-\frac{1}{p}-1)La}-e^{-ru}e^{rl-rpLa}\right]$$

$$I = \frac{aP}{(1-e^{rLa})}\left[e^{-ru}e^{-rpLa}-e^{ru}e^{-rLa\,p-1)}+e^{-ru}-e^{r(\frac{1}{a}-\frac{1}{p}-1)La}-e^{-ru}e^{rL(1-pa)}\right]$$

Where $p = a = 1$

$$I = \frac{aP}{(1-e^{rLa})}\left[e^{-ru}(e^{-rpLa}-1)+e^{ru}(e^{-r(\frac{1}{a}-p-1)}-1)\right]$$

$$I = aP\left(\frac{e^{-ru}(e^{-rpLa}-1)+e^{ru}(e^{-r(\frac{1}{a}-p-1)La}-1}{1-e^{rLa}}\right) \quad (3.3)$$

SINGLE CELL

The Capacity of one cell means $a = 1$ ad there is no inter cell interference and intra cell interference than equation (3.2) is given as [4].

$$C(1) = \frac{1}{rL}\int_{\frac{-rL}{2}}^{\frac{rl}{2}} Log_2\left(1+\frac{Pe^{-|v|}}{\sigma^2}\right)dv \quad (3.4)$$

MULTI CELL

For infinite number of cell means $a = 0$ the capacity formula equation (3.2) of path loss can be represented as

$$C(0) = \frac{1}{rL}\int_{\frac{-rL}{2}}^{\frac{rl}{2}} Log_2\left(1+\frac{P}{\frac{2P}{rL}\left(1-e^{\frac{-rL}{2}}\cosh(u)\right)+\sigma^2}\right)dv$$

3.2 Assume P is given by 1, γ rangers from 0-0.2, L is taken as 250, 500, 1000 , and σ^2 is 10^{-5} [4].

In Figure 1 plot of equation 3.4 is shown for the most likely values of length that can be used practically. We consider three lengths (250,500,1000 m) and discussed the effect of attenuation factor with respect to capacity. For L=250 m we obtain the comparatively best response other than two length which are 500 m and 1000 m. The reason of referring this is best response lies in the fact that capacity decreases slowly with respect to attenuation.

For L=500 m the response obtain is intermediate.

For L= 1000 m the Capacity decreases too rapidly compare to the other two.

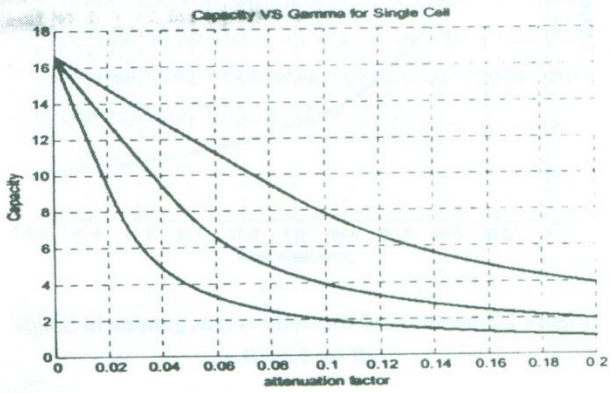

Figure 1 Simulation of Capacity versus gamma is Single cell for L=250, 500, 1000m

As the topic of research is mathematical analysis of design parameters we prefer L=500m due to following reason.

Although the response obtained for L=250 m was better than L=500 m but due to the economic constraints it is not feasible to install a base station at every 250 m.

In L=1000 m the cost reduced significantly but capacity decreases twice as rapidly as for L=500 m. This reduction of capacity cannot be tolerated in practical systems.

Another reason for taking L=500 m is that it is possible to provide a better capacity at affordable cost. By taking optimum length L=500 m in the single cell environment, plot capacity for multi cell environment using the same length. As oppose to the single cell even capacity for multi cell environment increases non-

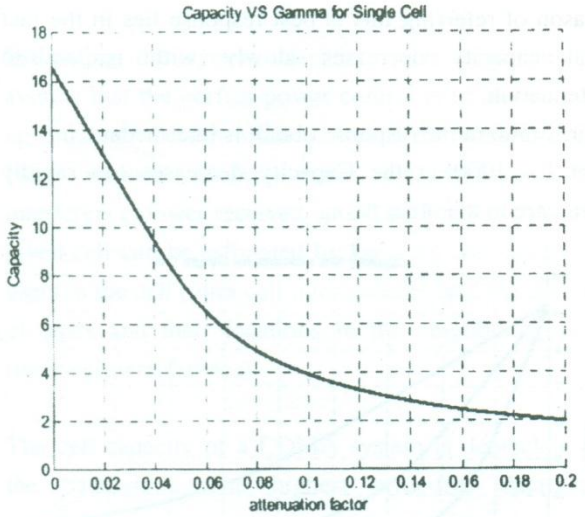

Figure 2 Simulation of Capacity versus gamma in Single cell for L=500m

linearly to a certain lirnit with the increase of attenuation factor. After a particular point the values of capacity almost become constant.

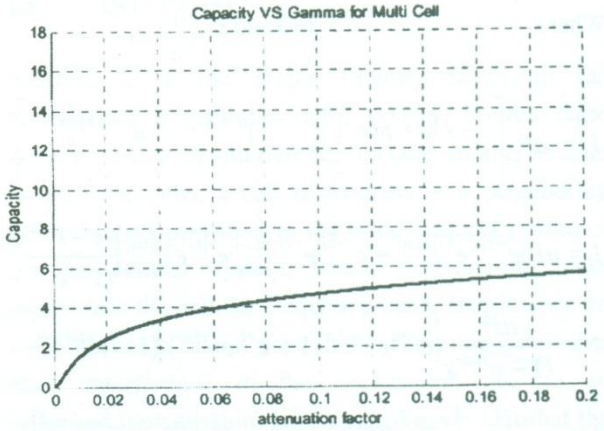

Figure 3 Simulation of Capacity versus gamma in Multi cell for L=500m

For above discussion it can be concluded that if the channel is at its peak the multi cell approach should be sought. The reason for preferring multi cell in practical situation is it's inherent to less power utilization capability. It is preferred in the urban areas because we can't assign a single frequency to a large area due to congestion.

The figure 4 shows the combination of two cells environment Single cell and Multi cell for an optimum

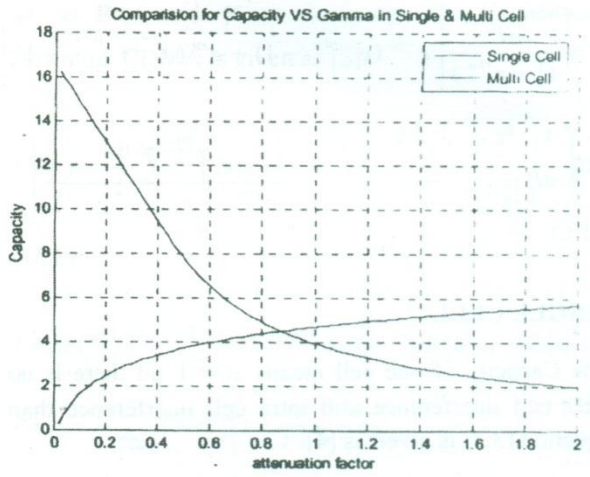

Figure 4 Simulation of Capacity versus gamma in Single cell and Multi Cell for L=500 m

Length L=500 m. In a single cell the capacity is initially high but it decay with the increase in attenuation factor. Capacity of multi cell is gradually increases as the gamma increases. As seen from the graph the intersection point is called critical point denoted by r_0, where we have three conditions. Before r_0, there is no advantage of using multi cell as single cell offer better capacity. But after r_0, single cell capacity decay rapidly where increase in capacity is observed in the case of multi cell. At r_0, ' The response of both the curve is same but by taking cost factor into account single cell should be preferred.

4. CONCLUSION

In this paper, simulation of single cell & multi cell network of CDMA downlink scheme is discussed. For Single cell, effect of different lengths on capacity with respect to attenuation factor is analyzed. Using the analysis results from the optimum length of 500m. Moreover the contribution of same length is analyzed for Multicell environment. Finally the comparison of Single & Multi cell for this length (L=500 m) is taken and comparison of Single cell and Multi cell the critical point which is represented by r_0, is crucial to establish the following three conditions, before critical point, where there is no benefit of utilization of Multi cell as the capacity response of single cell is better. After critical point, Single cell is adversely affected by increase an attenuation where as Multicell offers a better solution. At critical point, although both the system provide the same result but due to economic limitation Single cell should be favored.

REFERENCES

[1] Kizito Tshilumba Kasengulu, "About the capacity of DS spread spectrum CDMA Cellular System", Berocan inc., Montreal pp I

[2] Kevin Kong-Hang Chan, "An Analysis of Wireless High-speed Data Services for Cellular CDMA Systems", submitted to the University of Waterloo, Ontario, December 2002, pp 5.

[3] Debbah, Merouane Capacity of a downlink MC-CDMA multi-cell network ICASSP 2004, 29th IEEE International Conference on Acoustics, Speech and Signal Processing, May 17-21, 2004, Montreal, Canada, pp 761-764 vol.4

[4] Debbah, Merouane Downlink CDMA: to cell or not to cell EUSIPCO 2004, 12th European Signal Processing Conference, September 6-10,2004, Vienna, Austria

[5] Bonneau, Nicolas; Debbah Merouane; Altrman, Eitan Spectral efficiency of CDMA downlink cellular networks with matched filter EURASIP Journal on Wireless Communications and Networking, Volume 2006, pp 1-10

ISSN 1665-8607

CONTENTS

VOLUME 8 NO. 1&2 JAN-DEC-2007

Published by

Directorate of Research & Publication, Quaid-e-Awam University of Engineering, Science & Technology, Nawabshah Sindh-Pakistan
(Phone # 92-244-9370362, Fax# 92-244-9370362) email:sfaizsamo@yahoo.com

Composed & Printed by

Soomro Computer Composers & Printers Nawabshah, Golwala Complex Katchehry Road Nawabshah
Sindh-Pakistan (Phone # 92-244-291511, Cell # 92-333-7014550) email:sagersindh@gmail.com